Microwave Laboratory
W. W. Hansen Laboratories of Physics
Stanford University
Stanford, California

Semi-Annual Report

for the period

March – September 1974

submitted to

NASA - LANGLEY

Contract NSG-1012

INFRARED DIFFERENTIAL ABSORPTION FOR ATMOSPHERIC POLLUTANT DETECTION

by

Professor R. L. Byer
Applied Physics Department
Stanford University
Stanford, California

M. L. Report No. 2357

October 1974

TABLE OF CONTENTS

INFRARED DIFFERENTIAL ABSORPTION FOR ATMOSPHERIC POLLUTANT DETECTION

I. INTRODUCTION

This first semi-annual report summarizes the progress made to date in the generation of tunable infrared radiation and its application to remote pollutant detection by the differential absorption method.

At the Laser Radar Conference in Sendai, Japan held recently, it was recognized that future remote pollutant measurements depended critically on the availability of high energy tunable transmitters. Furthermore, due to eye safety requirements, the transmitted frequency must lie in the 1.4 μm to 13 μm infrared spectral range.

Recent experiments by Walther et al., at the University of Cologne in Germany[1] and by Grant et al., at S.R.I.[2] have shown experimentally that the differential absorption method offers the best potential for sensitive remote pollutant detection. There was general agreement at the Sendai conference that this is the case.

Our paper, describing progress in our high energy tunable coherent source was the only paper presented at the conference concerned with the generation of high energy tunable infrared radiation. A preprint of the paper[3] describing the 1.4 μm to 4.4 μm $LiNbO_3$ parametric oscillator is given in Appendix I.

Appendix II is a preprint of a review paper[4] on remote pollutant detection written for the ICO Meeting held in Tokyo just prior to the Sendai Meeting. This paper has been submitted to Opto-Electronics for publication.

II. DIFFERENTIAL ABSORPTION METHOD

We have given further consideration to pollutant measurement by the differential absorption method. Three areas of concern have been identified. They are required transmitted energy vs wavelength in the infrared due to the approximately λ^2 decrease in Mie backscatter with wavelengths between 1 μm and 10 μm; the decrease in scintillation in the infrared and the reduction in signal to noise ratio due to digitation noise.

The decrease in returned signal due to the λ^2 decrease in Mie scattering is being investigated in more detail theoretically. But at this time differential absorption measurements may be limited to wavelengths less than 5 μm with the present transmitter operating at 20 mJ pulse energy.

A review of scintillation studies seems to indicate the likely possibility of an alternate on and off resonance pulsed system as opposed to a double pulsed system. In the infrared, scintillation decreases in amplitude with increasing wavelength. Due to the high cost and difficult technology involved in a double pulse system we plan to carry out initial work with the alternate pulsed approach.

Recent advances in A to D converters has led to a 10 bit, 10 MHz system at a cost of under $10,000.[5] This A to D converter, followed by a buffer memory is fully capable of processing the return radar signal in conjunction with our PDP11E-10 computer. We feel that the 10 bit capability is essential if full sensitivity is to be obtained in the differential absorption measurements.

We are presently discussing possible additional support with the Electric Power Research Institute (EPRI) to aid in the purchase of the A to D converter for the data receiving system.

III. HIGH ENERGY WIDELY TUNABLE INFRARED SOURCE

We have successfully demonstrated the 1.4 μm to 4.4 μm $LiNbO_3$ parametric oscillator source. The important results are summarized in the preprint presented in Appendix I.

Our present effort lies in the evaluation of the 1.06 μm amplifier chain and operation of the oscillator at higher input energies. We expect to complete this work within the next two weeks.

Our schedule calls for the completion of the computer controlled oscillator stage by January 1975. We should be ready to initiate external pollutant measurements by early Spring.

The growth of (01·4) $LiNbO_3$ crystals has been carried out by three companies so that a commercial supply of these crystals should be available soon.

IV. DATA PROCESSING SYSTEM

The PDP11E-10 minicomputer was received in July. It is now fully operational with RT-11 and basic software. Recently we received the CAMAC interface crate and stepper motor controllers. A software program was completed which allows programing of stepper motors and D to A converters. We have demonstrated the capability by programing a stepper motor.

We are presently evaluating data display systems. Costs and capabilities range from $3,500 for a CAMAC controlled color TV display to over $25,000 for a full computer controlled random access color display.

At the Sendai conference C. Frush of NOAA presented a paper describing a computer compatable fast A to D converter with gain switching and buffer memory. We have called Dr. Frush and are more carefully evaluating his processor.

At this time, the specifications of Computer Labs. 10 bit A to D converter appear to be the best available. We hope to complete the evaluation of the available systems during the next two months.

V. MEASUREMENT PROGRAM

We have initiated design of a telescope receiving system and the necessary building modifications to install a receiver-transmitter system on the Microwave Laboratory roof. From our roof location probable targets for a future air pollution study are down-town Palo Alto (range ~1km), Stanford parking lot (range ~200 m) and the Stanford Steam Plant (range ~300 m). We also have numerous targets for topographical reflectors including Hoover tower (range 600 m), Eucalyptus trees (range 500 m) and the hills across the Bay (range ~10 km). We will more fully evaluate these potential targets as our measurement program begins. However, at this time the natural gas burning Stanford Steam Plant appears to be an ideal active source for future study.

REFERENCES

1. K.W. Rothe, U. Brinkman and H. Walther, Proc. VIII, ICPEAC, Beograd, (July 1973).

2. W.B. Grant, R.D. Hake. Jr., E.M. Liston, R.C. Robbins and E.K. Proctor. Jr., Appl. Phys. Letts. 24, p.550, (1974).

3. R.L Herbst, R.N. Fleming and R.L. Byer, "A 1.4 μm to 4 μm High Energy Angle Tuned $LiNbO_3$ Parametric Oscillator", Appl. Phys. Letts. (Nov. 1974).

4. R.L. Byer, "Remote Air Pollution Measurement", presented at ICO Conference, Tokyo, Japan, August 1974, (submitted for publication).

5. Computer Labs., North Carolina.

APPENDIX I

A 1.4 μm to 4.4 μm HIGH ENERGY ANGLE TUNED $LiNbO_3$ PARAMETRIC OSCILLATOR

R.L. Herbst, R.N. Fleming and R.L. Byer

ABSTRACT

We have operated a high gain, angle tuned, singly resonant $LiNbO_3$ parametric oscillator pumped directly at 1.06 μm by a Q-switched Nd:YAG laser. The oscillator angle tunes from degeneracy and operates over the entire 1.4 μm to 4.4 μm range. Output energies of greater than 1 mJ/pulse at 5 pps have been observed with a 15% energy conversion efficiency. The key to this device is the large $LiNbO_3$ crystals fabricated from new [01·4] grown boules. Crystals up to 15 mm diameter and 5 cm in length have been cut at the nominal 47° orientation. These crystals will potentially handle over 2J of optical energy at 1·06 μm.

A 1.4 μm to 4.4 μm HIGH ENERGY ANGLE TUNED $LiNbO_3$ PARAMETRIC OSCILLATOR

At present two methods are available for obtaining peak powers greater than several hundred watts of continuously tunable coherent radiation in the 1.5 to 4.5 μm region. These are parametric mixing and parametric oscillation. Since in parametric mixing two input wavelengths are needed one of which is tunable, mixing wavelengths have been limited primarily to the visible and near infrared where dye lasers provide the tunable component. Although high peak input powers are available efficient down conversion has not been realized because of problems of beam overlap and phase mismatch.[1,2,3] Parametric oscillators,[4-10] potentially efficient converters in the region, have been limited to low power or low efficiencies because of operation far from degeneracy, small crystal size or low crystal damage threshold.

We have recently studied a potentially high energy widely tunable infrared source. The device is an angle tuned, singly resonant $LiNbO_3$ parametric oscillator pumped by a Q-switched 1.06 μm Nd:YAG laser. The oscillator operates at room temperature and tunes the complete range of 1.4 μm to 4.45 μm. The key element in this device is the large $LiNbO_3$ crystals available by using a new [01·4] boule growth direction.

$LiNbO_3$ boules grown along the [01·4] axis[11] yield large diameter, strain free, high optical quality crystals. The boule axis lies 38° to the optic axis in the yz plane. Thus large parametric oscillator crystals can be fabricated at the nominal 47° phasematching angle desired for a 1.06 μm pumped parametric oscillator. To date we have grown fourteen boules and have fabricated oscillator crystals 1.5 cm diameter by 5 cm long. Using SiO_2 anti-reflection coatings, these $LiNbO_3$ crystals have operated in the parametric oscillator at greater than 2 J/cm^2 energy density without damage. For our 20 nsec Q-switched pulse the

corresponding surface intensity is 100 MW/cm^2.

The boules are grown by the Czochralski method at the congruent melt composition using seeds with a known [01·0] direction. After annealing, the boules are poled to maximize the effective nonlinear coefficient. Since $d_{eff} = d_{31} \sin(\theta + \rho) + d_{22} \cos(\theta + \rho) \sin 3\varphi$ where θ is the phasematching angle, ρ the double refraction angle and φ the orientation with respect to the [11·0] direction, and d_{31} and d_{22} are known to be of opposite sign,[12] the effective nonlinear coefficient is maximized for propagation in the second and fourth yz quadrants. For $|d_{31}| = 6.25 \times 10^{-12}$ (m/V) and $|d_{22}| = 3.3 \times 10^{-12}$ m/V , $d_{eff} = 6.88 \times 10^{-12}$ m/V for $\theta = 47^\circ$ and $\rho = 0.04$ rad. Thus the effective nonlinear coefficient is slightly larger at $\theta = 47^\circ$ than that for $\theta = 90^\circ$.

The experimental setup is shown in Fig. 1a. The pump source is a low energy flashlamp pumped Nd:YAG laser operating at 1.06 μ at 10 pps. The laser is electro-optic Q-switched with output energies of up to 20 mJ in a 20 ns pulse. Operation is limited to a TEM_{oo} mode with an internal aperture but no effort was made to limit the spectral bandwidth. Figure 1b shows a photograph of the $LiNbO_3$ oscillator with 1 cm diameter by 5 cm crystal within the oscillator cavity.

The laser output having a 780 μ spot size is incident directly on the oscillator cavity without collimation or mode matching. For operation over the entire tuning range two sets of parametric oscillator mirrors were used. However, broadband mirror coatings covering the 1.4 to 2.1 μm region will allow tuning over the entire range from 1.4 μm to 4.4 μm with one set of optics. The oscillator cavity consists of two long radius or flat mirrors spaced by 7 cm. The $LiNbO_3$ oscillator crystal was held in a copper block at room temperature. No attempt was made to stabilize the crystal temperature and small variations in oscillator wavelength with changes in room temperature

occurred. For these initial experiments these variations were not a problem but for long term stability an oven stabilized to $\pm .1^{\circ}C$ will be required.

Figure 2a shows the calculated tuning curve for the $LiNbO_3$ parametric oscillator using Hobdens and Warner's index of refraction relations.[13] Also plotted are the measured data points. The triangular points were taken with a 2 m high reflector input mirror and a flat 4% output coupler. These were standard mirror coatings centered at 1.8 μm. The single circle data point at 1.4 μm was taken with standard 1.32 μm Nd:YAG laser optics consisting of a high reflector flat input mirror and a flat 10% output coupler. The oscillator tuned continuously over the entire range. Tuning of the oscillator beyond the 4.4 μm point was limited by the inability to reach threshold due to increasing infrared absorption of the idler wave. The oscillator threshold, measured near 1.9 μm was 4 mj corresponding to 1.5×10^5 watts of pump power. The measured gain bandwidth varied from 3 cm^{-1} near 1.5 μm to 23 cm^{-1} near degeneracy.

Because of the large double refraction in $LiNbO_3$ at the 47° crystal angle, a large pump beam spot size is needed to reduce the effect of pump beam walk-off on parametric gain. An estimate of the pump beam spot size can be obtained using[14]

$$w_3 = \frac{1}{\sqrt{2\pi}} \rho \ell \qquad (1)$$

where ρ is the double refraction angle. For a 5 cm $LiNbO_3$ crystal at 47° with $\rho = 0.04$ radians, $w_3 = 800\ \mu$. Using higher power lasers and maintaining constant intensity the spot size increases such that the parametric gain approaches the plane wave limit given by[15]

$$G = \sinh^2 \Gamma \ell \qquad (2)$$

where

$$\Gamma^2 = \frac{2\omega_1\omega_2|d|^2}{n_1 n_2 n_3 \epsilon_o c^3} \frac{P_3}{A_3} \qquad (3)$$

and ℓ is the crystal length and $A_3 = \pi w_3^2/2$. At degeneracy we have

$$\Gamma^2 = 2.3 \times 10^{-2} \frac{P_3}{A_3} \left(\frac{MW}{cm^2}\right) cm^{-2}$$

Thus for pumping near the damage intensity threshold of 80 MW/cm^2 with large spot size beams, single pass gains of $G = 1/4\ e^{2\Gamma\ell} = 1.17 \times 10^6$ are possible in 5 cm crystals. These gains are approximately that required for superradiant operation and illustrate the high gains possible in parametric devices.

An important aspect of using a large spot size to pump a parametric oscillator that is often overlooked is the ability to use tilted etalons inside the oscillator cavity with low insertion loss. For a tilted etalon the insertion loss is given by[16]

$$\ell = \frac{R}{(1-R)^2}\left(\frac{4\alpha d}{nw}\right)^2 \qquad (4)$$

where α is the tilt angle, d the etalon thickness, R the etalon reflectivity, and w the beam radius. The requirement for large spot sizes at the resonated wave is apparent. Figure 2b shows the spectral output of the oscillator with a 2 mm thick, finesse of ten etalon inside the oscillator cavity. The linewidth of the individual etalon modes is less than 0.1 cm^{-1} and is not resolved by the spectrometer. By scanning the etalon angle we tuned an individual mode over many free spectral ranges without increasing the cavity loss. The amplitude envelope of the etalon modes is determined by gain linewidth of the parametric oscillator.

Figure 3 demonstrates the oscillator output stability. Figure 3a shows that the peak-to-peak fluctuation of the total oscillator output over a five minute period is less than 3% as monitored by an Eppley thermopile with a one second time constant. During this measurement the oscillator operated at 5 pps with 1 mJ per pulse output energy. Figure 3b shows 1000 consecutive output pulses at 20 pps. The oscillator operated 7 mW average power with a peak to peak stability of 3%. Since the InSb detector did not resolve the 20 nsec pulse, the oscilloscope trace is a measure of output energy stability with a 1 μsec time constant.

In conclusion, we have demonstrated a widely tunable infrared source that can be rapidly and conveniently angle tuned over the entire 1.4 μm to 4.4 μm range. It is significant that the source requires only one set of optics and a single $LiNbO_3$ crystal to tune the entire range. Conversion efficiencies of 15% and operating stability of better than 3% have been observed. The availability of large 15 mm diameter by 5 cm long, 47° cut $LiNbO_3$ crystals allows operation of the oscillator at up to 2J of 1.06 μm input pulse energy. The large oscillator mode radius allows the use of a tilted etalon for line narrowing without significant reduction of output power.

Finally, it should be noted that the oscillator covers more than one octave of tuning range so that its frequency can be extended into the visible and ultraviolet by second harmonic generation in $LiNbO_3$ and $LiIO_3$ and still maintain complete spectral coverage. Frequency extension into the infrared is most easily done by mixing the signal and idler waves in semiconductor nonlinear crystals such as $AgGaSe_2$[17] and CdSe[18] which phasematch over a 3 μm to 18 μm and 10 μm to 25 μm range. The high output power of the $LiNbO_3$ tunable source insures that the nonlinear doubling and mixing steps will proceed with good efficiency.

ACKNOWLEDGEMENTS

We wish to acknowledge support for this work under contracts with NSF-RANN, NASA and AEC.

REFERENCES

1. C.F. Davey and L.O. Hocker, Appl. Phys. Letts. 18, p.58, (1971).

2. D.W. Meltzer and L.S. Goldberg, Optic Comm. 5, 209, (1972).

3. C.D. Decker and F.K. Tittel, Appl. Phys. Letts. 22, p.411, (1973).

4. L.B. Kruzer, Appl. Phys. Letts. 15, 263, (1969).

5. E.O. Ammann and J.M. Yarborough, Appl. Phys. Letts. 17, 233, (1970).

6. D.C. Hanna, B. Luther-Davies, H.N. Rutt and R.C. Smith, Appl. Phys. Letts, 20, 1,(1972).

7. A.J. Campillo, IEEE J. Quant. Elect. QE-8, 809, (1972).

8. D.C. Hanna, B. Luther-Davies and R.C. Smith, Appl. Phys. Letts. 22, 440, (1973).

9. R.W. Wallace, Appl. Phys. Letts. 17, 497, (1970).

10. J.M Yarborough, J. Falk and E.O. Ammann, "Tunable Laser Research", GTE Sylvania Final Report prepared for ONR under Contract N00014-72-C-0245, (May 1973).

11. R.L. Byer, R.L. Herbst, R.S. Feigelson and W.L. Kway, "Growth and Application of [01·4] $LiNbO_3$", to be published.

12. J.E. Bjorkholm, Appl. Phys. Letts. 13, 36, (1968).

13. M.V. Hobden and J. Warner, Phys. Letts. 22, 243, (1966).

14. G.D. Boyd and D.A. Kleinman, J. Appl. Phys. 39, 3597, (1968).

15. R.L. Byer, "Optical Parametric Oscillators", to be published in Quantum Electronics, H. Rabin and C.L. Tangs, eds. Academic Press, 1974.

16. M. Hercher, Applied Optics, 8, 1103, (1969).

17. R.L. Byer, M.M. Choy, R.L. Herbst, D.S. Chemla and R.S. Feigelson, Appl. Phys. Letts. 24, 65, (1974).

18. R.L. Herbst and R.L. Byer, Appl. Phys. Letts. 19, 527, (1971).

FIGURE CAPTIONS

1. a) Schematic of experimental arrangement showing the electro-optic Q-switched 1.06 μm Nd: YAG laser and $LiNbO_3$ parametric oscillator.
   b) Photograph of the singly resonant $LiNbO_3$ parametric oscillator with a 1 cm by 5 cm crystal within the oscillator cavity.

2. a) Calculated parametric oscillator tuning curve and accurately measured wavelength vs crystal angle points. The entire tuning range to the circles was continuously scanned using a single 15 mm × 5 cm oscillator crystal.
   b) Spectral output of the oscillator with a tilted etalon. The linewidth of individual etalon modes is less than 0.1 cm^{-1} and is not resolved by the spectrometer. The amplitude of the etalon modes shows the gain envelope of the parametric oscillator.

3. a) Average output stability of the oscillator operating at 5 pps, 1 mJ/pulse for five minutes with an Eppley thermopile,
   b) Peak to peak stability showing 1000 pulses at 20 pps. The average and peak output fluctuations are less than 3%.

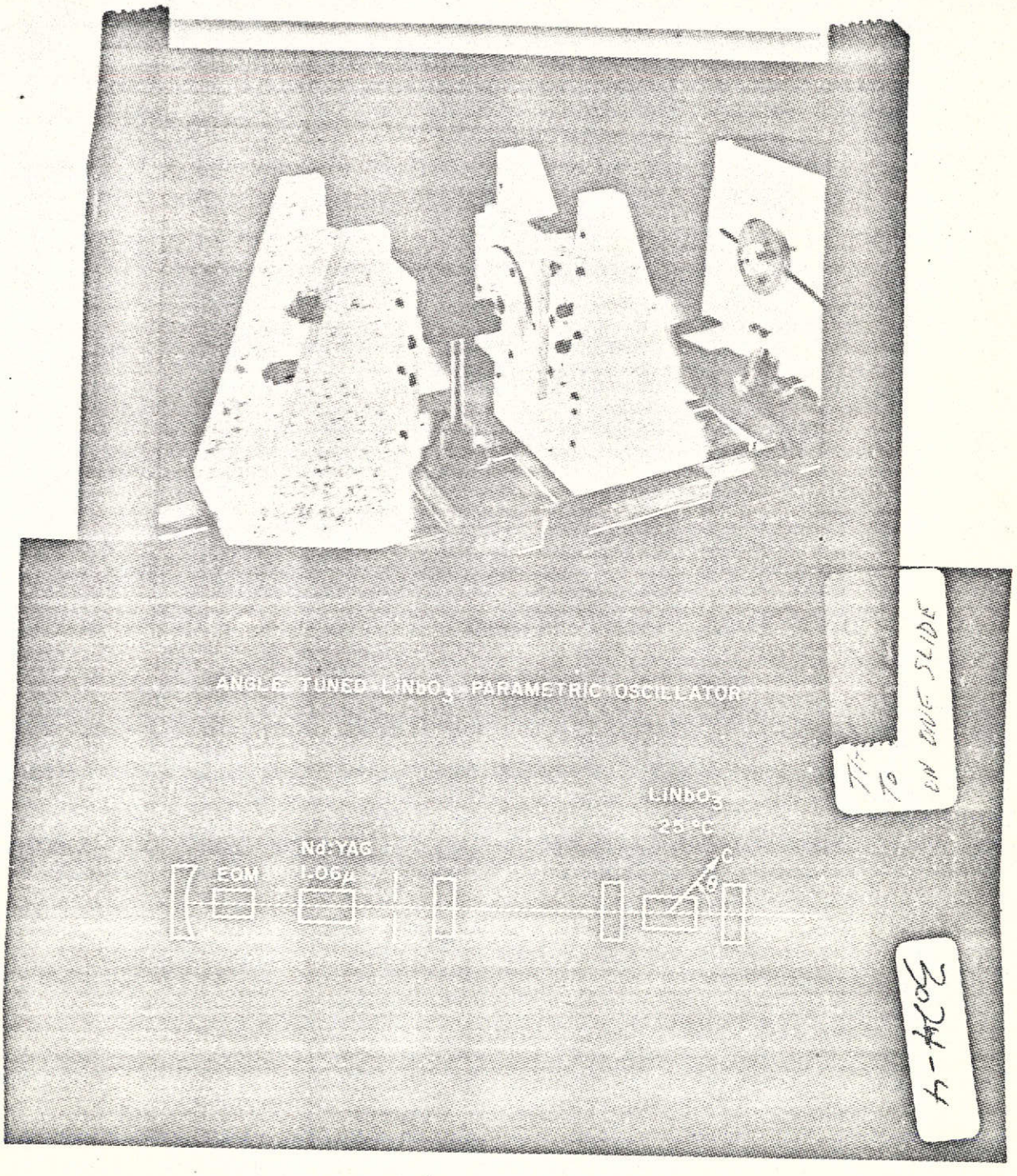

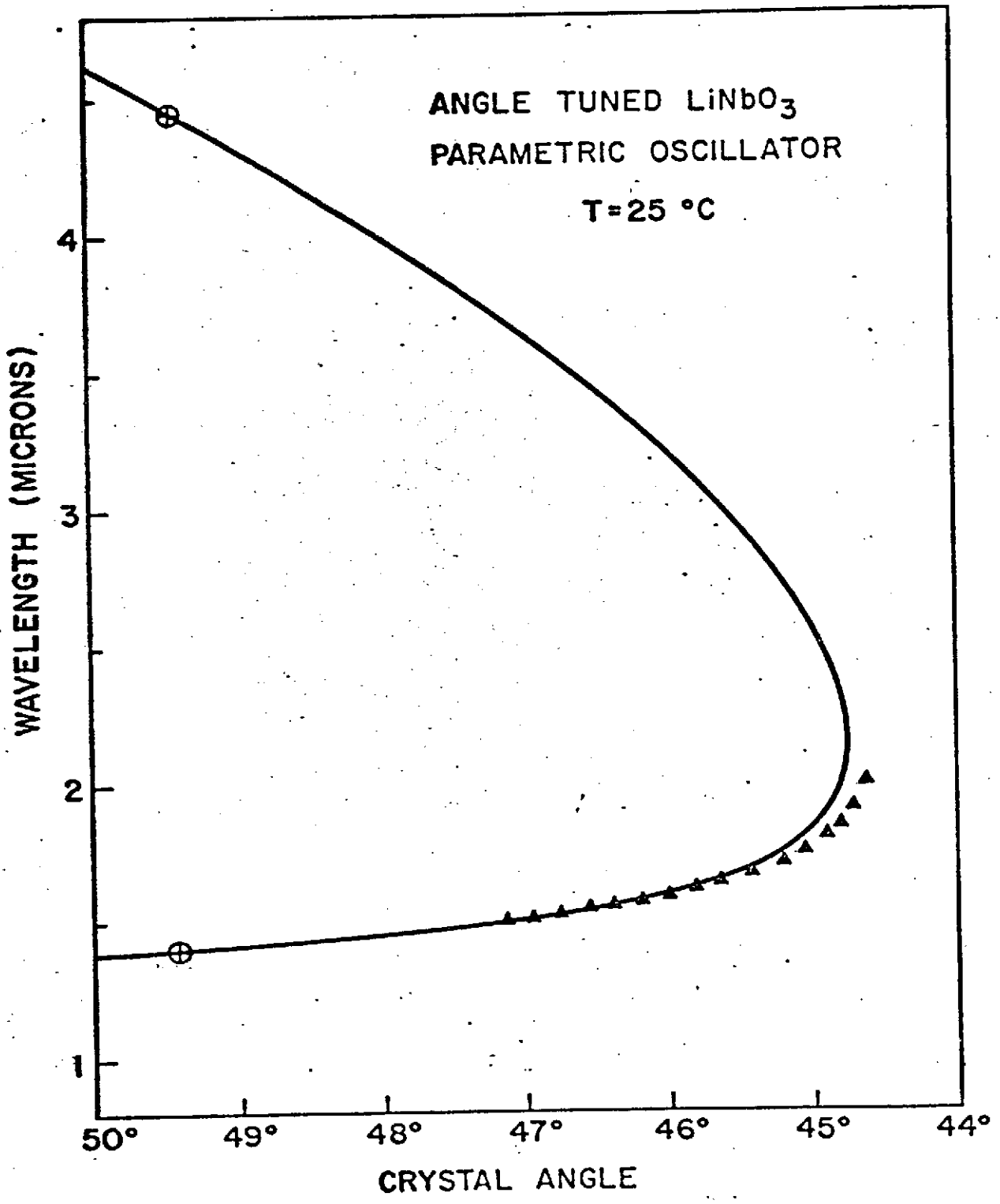
ANGLE TUNED $LiNbO_3$
PARAMETRIC OSCILLATOR
T=25 °C
WAVELENGTH (MICRONS)
4
3
2
1
50°
49°
48°
47°
46°
45°
44°
CRYSTAL ANGLE

FIGURE 2a

OSCILLATOR OUTPUT WITH 2mm ETALON
$\delta\tilde{\nu}$=10
1.7736
1.7730
1.7724
1.7718
1.7712
1.74 cm-1

FIGURE 2b

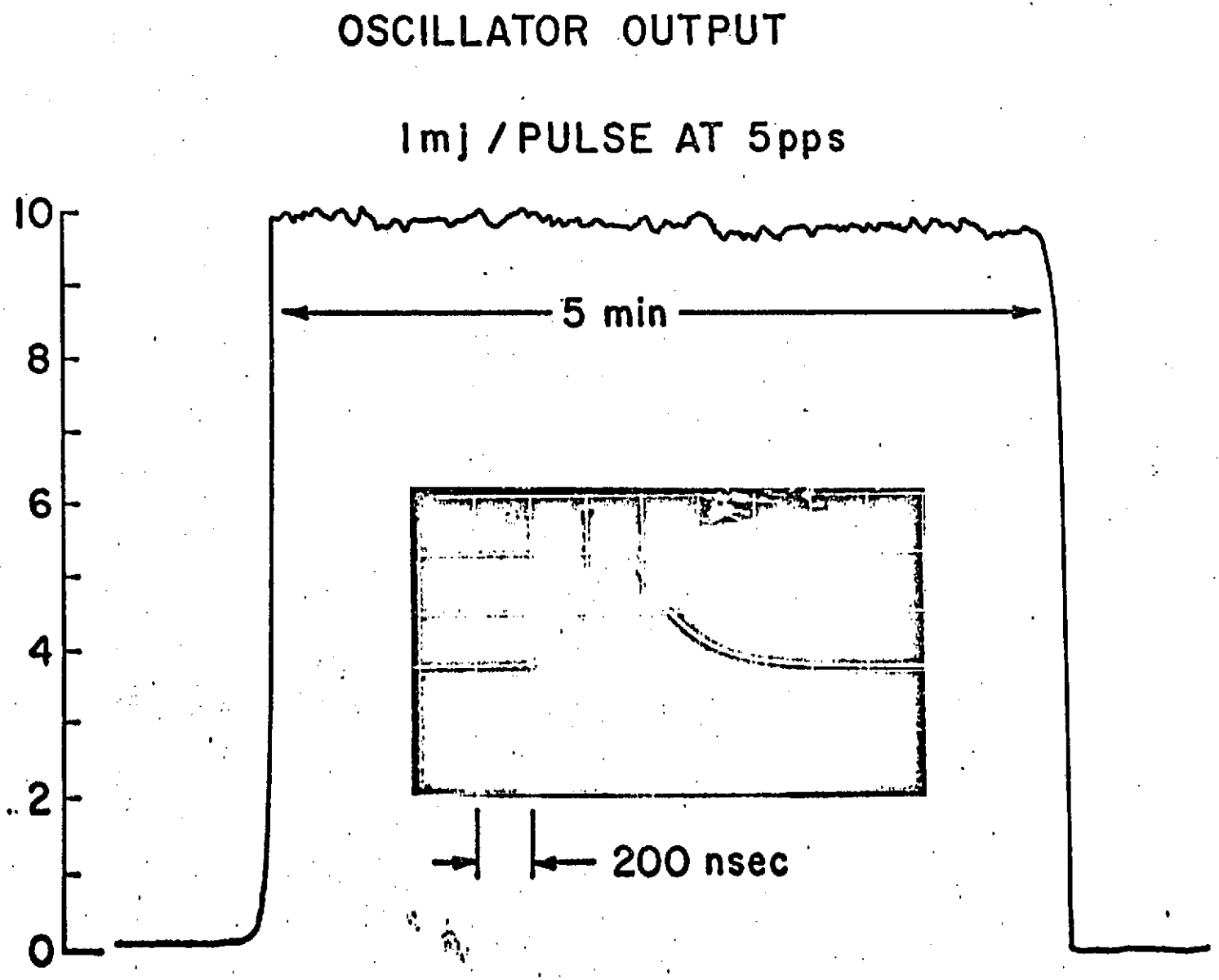

FIGURE 3a and 3b

APPENDIX II

REMOTE AIR POLLUTION MEASUREMENT

by

Robert L. Byer
Professor of Applied Physics
Stanford University
Stanford, California

REMOTE AIR POLLUTION MEASUREMENT

by

Robert L. Byer
Professor of Applied Physics
Stanford University

(Received August 29, 1974)

ABSTRACT

The availability of high energy tunable laser sources has extended the possibilities for remote air pollution measurement. This paper presents a discussion and comparison of the Raman method, the resonance and fluorescence backscatter method, long path absorption methods and the differential absorption method. A comparison of the above remote detection methods shows that the absorption methods offer the most sensitivity at the least required transmitted energy. Topographical absorption provides the advantage of a single ended measurement, and differential absorption offers the additional advantage of a fully depth resolved absorption measurement. Recent experimental results confirming the range and sensitivity of the methods are presented.

Future widespread use of remote pollution monitoring will probably be limited to the infrared to interact with molecular spectral bands and to meet eye safety requirements.

REMOTE AIR POLLUTION MEASUREMENT

I. INTRODUCTION

A number of review articles on air pollution measurements have already been published.[1-6] However, recent advances in tunable laser technology coupled with experimental verification of remote sensing methods bring remote pollution measurements very close to a practical state. This paper reviews the field of remote pollution measurement and indicates the requirements for tunable laser transmitters.

The adverse effects of polluted air on human health is well established and an estimation of the cost savings for human health alone in the United States is over one billion dollars for a 50% air pollutant reduction.[7] The Environmental Protection Agency has established maximum pollutant levels and goals for future reduction in pollutant levels. To meet these standards, accurate sensitive measurement methods must be established. Major pollutants of interest include ozone, nitrogen oxides, carbon monoxide, sulfer dioxide and hydrocarbon compounds. These pollutant molecules are present in urban atmospheres in concentrations from .01 ppm to over 10 ppm.[8] Remote pollutant measurement methods must have measurement sensitivities in this range if they are to be useful for atmospheric monitoring. In addition, the detection methods must be capable of monitoring molecular vapors. Both Raman scattering and infrared absorption on molecular vibration bands satisfy this last requirement. The detection sensitivity inherent in absorption and the regard for eye safety requirements probably limit future remote pollution detection methods to the infrared spectral region.

A. Historical Overview

Historically lasers were first used in radar type remote sensing applications. The acronyn LIDAR for Light Detection and Ranging was applied to laser ranging systems. In 1963 Fiocco and Smullin[9] recorded backscattered echoes from turbidity in the upper atmosphere and Ligda[10] measured backscatter from the molecular atmosphere and haze. Since that early work considerable effort has gone into LIDAR development and applications. The remote pollutant detection methods considered in this paper are an extension of LIDAR and therefore work in LIDAR and its applications are of interest. Early reviews and discussions of LIDAR are given by Inaba, Kobayashi and Ichimura[11], Collis[12], Kent and Wright[13] and Collis.[14] More recent reviews including discussions of the wide ranging applications of LIDAR are given by Derr and Little[2], Strauch and Cohen[15], Collis and Uthe[16], Allen and Evans[17], Hall[18] and Collis and Russel.[19] The field has grown rapidly and has laid much of the ground work for remote pollution detection methods.

Using the then available fixed frequency laser sources Raman scattering was first used to detect molecular constituents of the atmosphere by Leonard[20], Cooney[21] and Melfi et al.,[22] Later Inaba and Kobayshi[23] discussed pollutant detection by Raman scattering and presented experimental work showing the detection of SO_2 and CO_2 molecules.[24] Remote detection by Raman scattering has the advantage of using a fixed frequency laser source which can operate in the visible or violet spectral region where photomultiplier detectors are available. Unfortunately, the molecular detection sensitivity possible by remote Raman scattering is not adequate for trace contaminant measurements. However, considerable effort has gone into using Raman scattering for monitoring water vapor profiles[25] and major components of the atmosphere.[26,27] Recently

Inaba and Kobayshi[4] reviewed Laser-Raman Radar and its applications to remote monitoring. Remote detection by Raman backscattering is discussed in Section II.

The availability of tunable laser sources opened additional remote pollutant detection possibilities.[1] They include long path absorption, detection of resonance fluorescence and differential absorption. The advantages of these detection methods is the increased molecular detection sensitivity due to the large absorption and fluorescence cross sections. In addition, absorption and fluorescence methods can be used for the detection of both molecular and atomic species.

Using multiple line laser sources Hanst and Morreal[28] and Snowman and Gillmeister[29] investigated the possibility of pollutant detection by long path absorption. The low required transmitted powers for long path absorption also allows the use of tunable cw infrared diode laser sources[3] and Raman spin flip laser sources.[30] In addition detection sensitivity can be improved by heterodyne techniques.[31] Although long path absorption provides the most sensitivity of any remote detection method it has the disadvantages of being double ended and lacking depth resolution. The first disadvantage can be overcome by obtaining a return signal from topographical targets but at an increase in required transmitter power. Both disadvantages are overcome by the differential absorption method first discussed by Schotland[32] and analyzed in detail by Measures and Pilon[5] and Byer and Garbuny.[33]

The differential absorption method provides a fully depth resolved absorption measurement of pollutant concentration vs range by using the molecular and Mie particle scattering as a distributed reflector. The required transmitter power,

signal to noise ratio of the returned signal, and sensitivity of the differential abosrption method is discussed in detail in Section II.

The improvements in tunable laser sources has proceeded rapidly so that tunable sources are now considered available for remote pollution measurements. Without the use of tunable laser sources, remote air pollution detection is limited to LIDAR and Laser-Raman methods neither of which is adequate for the measurement of weakly concentrated molecular pollutants. Tunable laser sources increase remote pollutant measurement possibilities to include resonance fluorescence and the absorption methods which do provide the capability of sensitive remote detection. The importance of tunable laser sources is evident in discussion of remote detection methods presented in Section II.

Table I lists remote pollution detection methods and provides an outline of the measurement methods discussed in Section II.

B. Atmospheric Parameters

The atmosphere attenuates a transmitted optical beam by elastic and inelastic scattering and by absorption. Some of the scattered light returns to a receiver to provide a signal from which atmospheric properties can be determined. In general an incident beam of intensity I_o propagating through the atmosphere is attenuated exponentially or

$$I = I_o e^{-\alpha_A r} \tag{1}$$

where I is the transmitted intensity over a distance r and α_A is the atmospheric volume extinction coefficient which is composed of a sum of terms

$$\alpha_A = \alpha_R + \alpha_{MIE} + \alpha_{ABS} \tag{2}$$

TABLE I

REMOTE AIR POLLUTION MEASUREMENT METHODS

ELASTIC SCATTERING
Rayleigh
Mie
INELASTIC SCATTERING
Raman
Resonance fluorescence
Fluorescence
ABSORPTION
Long path - retroreflector
Long path - topographic target
Differential absorption

where α_R , α_{MIE} and α_{ABS} are the Rayleigh, Mie and absorption extinction coefficients. The Rayleigh extinction coefficient is due to molecular scattering and can be calculated as a function of altitude for known atmospheric molecular densities. Mie scattering is due to particulates and aerosols in the atmosphere and is highly variable in both particulate size, wavelength and particle distribution. For identical molecules of density N , the volume extinction coefficient can be written in terms of a cross section $\alpha = \sigma N$ where σ is the total cross section (cm^2) for the optical interaction with the molecule or particle.

In general the scattering of light from molecular or particulate matter is not isotropic. The cross section is then specified by the differential cross section $\sigma(\theta, \varpi) = \frac{d\sigma}{d\Omega}$ where θ is the scattering angle and ϖ is the polarization angle. For isotropic scattering the scattering cross section per unit solid angle is $d\sigma/d\Omega = \sigma/4\pi$. For backscattering ($\theta = \pi$) the volume backscatter coefficient $\beta = N\sigma(\pi)$.

For molecular Rayleigh scattering the differential cross section is[34]

$$\frac{d\sigma_R}{d\Omega} = \frac{\pi^2(n^2 - 1)^2}{3\lambda^4 N^2} (\cos^2\theta \cos^2\varphi + \sin^2\varphi) \qquad (3)$$

where n is the refractive index, N the density and λ the wavelength. For unpolarized light the angular factor averaged over ϖ reduces to $(\cos^2\theta + 1)/2$. Finally, for backscattering ($\theta = \pi$) the Rayleigh backscatter coefficient is uniquely related to the volume extinction coefficient by

$$\beta_R = \frac{8\pi}{3} N \sigma_R(\pi) \qquad (4)$$

so that it is possible to determine N by Rayleigh backscattering.

In the above discussion the Raman volume extinction coefficient has been neglected since it is at least an order of magnitude less than the Rayleigh extinction coefficient. However, for reference and later use, the Raman differential cross section on resonance is given by[35,36]

$$\frac{d\sigma_{RAM}}{d\Omega} = \frac{h\,\omega_L\,\omega_S^3\,\Gamma_{RAM}\,\chi''_{RAM}}{\pi\,c^4} \qquad (5)$$

where ω_L and ω_S are the laser and Stokes frequencies, Γ_{RAM} is the half width of the Raman line and χ''_{RAM} is the imaginary part of the Raman susceptibility. A list of Raman frequency shifts and cross sections is given by Inaba and Kobayshi.[4] The differential Raman scattering cross section is approximately 10^{-30} cm^2/sr for diatomic molecules.

The large variation in size, density distribution and properties of atmospheric aerosols preclude an accurate calculation of the Mie scattering cross section. However, because of its importance in the differential absorption method, it is useful to summarize the properties of light scattering from atmospheric particulates and aerosols. Scattering from particulates is characterized by the size parameter $\alpha = 2\pi r/\lambda$ where r is the particle radius. The ratio of scattering cross section $\sigma(n,\alpha)$ to geometric cross section is

$$k_M = \frac{\sigma_M(n,\alpha)}{\pi\,r^2}$$

For a uniform concentration of spherical particles the volume extinction coefficient is $\alpha_{Mie} = \pi r^2 k_M(n,\alpha)N$. The factor k_M can be calculated in

terms of an infinite series as first obtained by Mie.[37] Mie scattering has been treated by van de Hulst,[38] Kerker[39] and Born and Wolf,[40] and computer calculations have been used to investigate the detail properties of Mie scattering.[41] An example of the rapidly varying scattering amplitude as a function of α is given by Strauch and Cohen.[15]

In the atmosphere the particle sizes are distributed and a functional dependence for the density dependence on radius $N(r)$ is needed to evaluate the total scattering. Junge[42] proposed the distribution $dN(r) = C\, r^{-(v+1)}\, dr$ for aerosol distributions in the atmosphere with $v \sim 3$. Elterman[43] has also evaluated the distribution of atmospheric aerosols. Fortunately, the complicated integrals over particle size and angular parameters necessary to calculate Mie scattering cross sections, can be avoided by the use of empirical relations. For example, the visibility and average extinction coefficient obey the relation[44,45]

$$V = \text{const}/\,\bar{\beta}$$

where V is the visibility and $\bar{\beta}$ is the average extinction coefficient over the range.

A useful empirical relation relating the Mie backscatter coefficient to visibility is given by[46]

$$\beta_{\text{Mie}} = \frac{3.91}{V}\left[\frac{0.55}{\lambda}\right]^{0.585V^{\frac{1}{2}}} \text{ km}^{-1} \qquad (6)$$

where λ is in microns and V is in kilometers. This expression is an approximation and may not hold under unusual atmospheric conditions. However, recent measurements[47,48] have shown that Eq. (6) does not apply to Mie scattering

with laser sources but with increased variation in backscattered signal compared to white light sources.

Extension of Eq. (6) into the infrared is questionable since the particulate size distribution decreases rapidly for particle sizes greater than 1 to 2 μm. However, the Mie backscatter coefficient has been recently calculated for aerosols, fog and rain conditions for wavelengths out to 10 μm.[49,50] The calculations show that β_{Mie} varies approximately as λ^{-2} in the infrared between 1 μm and 10 μm reaching 10^{-4} - 10^{-3} km^{-1} at 10.6 μm. Recent measurements using a CO_2 laser source[51] show that $\beta_{Mie} \sim 10^{-4}$ km^{-1} at 10.6 μm confirming the calculated values. For a more complete discussion of atmospheric scattering see Goody[52] and Kondratyev.[53]

The final parameter in the atmospheric volume extinction coefficient is absorption. In the ultraviolet spectral region atmospheric absorption is not serious for wavelengths longer than 2500 Å. Below 2500 Å absorption due to atmospheric oxygen becomes important with an absorption coefficient reaching 1 km^{-1} at 2450 Å. The scattering contribution to the volume extinction coefficient in this region is also significant being between 1 km^{-1} and 5 km^{-1} for visibilities of 10 km to 1 km.[1]

In the infrared absorption is the major contribution to the volume extinction coefficient. The atmospheric transmittance in the infrared has been subject of a number of investigations.[1,55,56] Within the infrared atmospheric windows the absorption loss over a 1 km pathlength is significant even under clear day conditions. For example, for a 5 km visibility, a relative humidity of 75% and an air temperature of 60°F, the absorption coefficients in the two infrared windows 2.70 to 4.20 μm and 4.40 to 6 μm are approximately 0.4 and 0.8 km^{-1}. The scattering coefficients are almost an order of magnitude less.

From this discussion we conclude that the atmospheric volume extinction coefficient is approximately 1-2 km^{-1} in the ultraviolet and visible and 0.5 km^{-1} in the infrared window regions. The magnitude of the extinction coefficient sets a maximum remote sensing range for a horizontal path of less than 10 km if significant transmitted beam attenuation is to be avoided.

Two other properties of the atmosphere are important in remote sensing. They are atmospheric scintillation and background signal levels during both daytime and nightime operating conditions. A large amount of work has gone toward the characterization of atmospheric spatial scintillation due to turbulence.[57] For the propagation of laser beams through the atmosphere spatial scintillation leads to beam distortion, displacement and angular variations. Hansen and Madhu[58] have considered laser beams reflected from a retroreflector target and have shown that atmospheric phase fluctuations at the retroreflector lead to angle scintillations of the beam. Dabberdt and Johnson[59] have recently studied the wavelength dependence and saturation characteristics of spatial scintillation.[59] As expected atmospheric scintillation is less for infrared than for visible wavelengths.[51]

Temporal scintillation of the atmosphere is also important in remote sensing. Previous work[55] shows that temporal scintillation is constant to near 20 Hz and then falls linearly to zero at near 200 Hz. For remote ranging with nanosecond pulses over microsecond round trip pulse range times the atmospher is essentially "frozen" and does not lead to pulse amplitude variations. For cw measurements or slow pulse repetition rate experiments, pulses must be averaged to reduce the 1 - 6% scintillation modulation of the transmitted beam.[55] Increasing the receiver aperture size also reduces the scintillation induced modulation.

Atmospheric background radiation is of concern in evaluation detector signal to noise and system receiving parameters. Background radiation includes elastic and inelastic backscattered radiation as well as natural background radiation. Here we assume that background signals from Rayleigh, Raman, Mie and fluorescence scattering can be estimated from previous discussions and consider only that due to natural sources.

The background power at the receiving mirror, due to an extended source filling the field of view, is[60]

$$P_B = T_\lambda \quad \Delta\lambda \; \Omega_m \; A_m \; B(\lambda) \tag{7}$$

where T_λ is the atmospheric transmittance at λ, $\Delta\lambda$ the optical bandwidth of the detection system, Ω_m the receiving mirror field of view and $B(\lambda)$ the spectral radiance of the background source. The spectral radiance of the clear daytime sky peaks in the visible due to scattered solar light at a value of approximately 10^{-2} Wcm^{-2} μm^{-1} sr^{-1}. In the infrared the spectral radiance again peaks due to thermal radiation near 13 μm at approximately 10^{-3} Wcm^{-2} μm^{-1} sr^{-1}.[60] Below 3000 Å the ozone absorption layer in the upper atmosphere screens the solar radiation thus producing an effective night condition. Eq. (7) shows that the background signal is reduced by decreasing the field of view, the acceptance bandwidth and the receiver area. For a shot noise limited detector, such as a photomultiplier, the background power must be kept less than the signal power to maintain sensitivity. However, for dark current limited detectors such as infrared photodetectors, the background power incident on the detector can be greater than the signal power without degrading the sensitivity. The upper limit on the received background power is determined

by background fluctuations or detector saturation. The filtering of unwanted background radiation is thus much less of a problem for infrared remote sensing than for visible sensing.

The final parameter of concern in remote sensing in the atmosphere is the eye safety problem due to the transmission of high peak power laser beams. Recently such concern has been quantified by the adoption of eye safety standards by the American National Standards Institute. The recommended eye safety Maximum Permissible Exposure (MPE) in the visible band, 0.4 μm to 0.694 μm is 5×10^{-7} J/cm^2, increasing linearly to 2.5×10^{-6} J/cm^2 at 1.06 μm and maintaining that level out to 1.4 μm. In the infrared range 1.4 μm to 13 μm the MPE is $0.56t^{1/4}$ J/cm^2, which yields 14×10^{-3} J/cm^2 for a pulse length t of 300 nsec. In the ultravoilet the MPE varies from 2×10^{-4} J/cm^2 at 0.310 μm to 3×10^{-6} J/cm^2 at 0.26 μm to 10^{-4} J/cm^2 at 0.20 μm. Between 0.31 μm and 0.40 μm the MPE is 10^{-3} J/cm^2.

The very low MPE in the visible region rules out the use of high energy pulse laser sources for remote measurement. Since all molecular absorption lines in the infrared lie beyond 1.4 μm, eye safety standards can be easily met by use of a small beam expanding telescope. Public safety and eye safety standards will become increasingly important as remote sensing measurements move from the research stage to practical applications in the open environment.

II. MEASUREMENT METHODS - A COMPARATIVE ANALYSIS

A. General Formulation

The remote pollutant measurement methods are listed in Table I. In this section a general formulation is presented for the analysis of the sensitivity, range, and S/N for the pollutant detection methods.

The backscattered signal from a target at range R is given by

$$P_r(R) = \left(\frac{\rho}{\pi}\right) K P_o \frac{A}{R^2} \exp\left[-2 \int_o^R \alpha_A(r)dr\right] \qquad (8)$$

where P_r and P_o are the received and transmitted powers, K is the optical system efficiency, A the area of the receiving telescope and (ρ/π) the effective reflectivity of the remote target. The transmitted radiation interacts with the pollutant molecules through the atmospheric volume extinction coefficient α_A defined in Eq. (2). Returned signals due to Raman, resonant fluorescence and fluorescence are included in the effective target reflectivity ρ/π. The strength of the returned signals by the inelastic scattering processes is related to the scattering cross section for the process. The depth of the atmosphere probed by backscatter methods is shown schematically in Fig. 1. The sampled depth ΔR is given by

$$\Delta R = \frac{c\tau}{2} \qquad (9)$$

where $\tau = \tau_p + \tau_d + \tau_F$ is the sum of the laser pulse width, τ_p, the detector integration time, τ_d, and the molecular fluorescence time τ_F. For Raman, ultraviolet fluorescence and differential absorption measurements τ_F is negligible and the sampled depth is set by either the laser pulse width or the detector integration time. Of course the particular sampled depth at range R is determined by the standard Radar time of flight measurement.

Table II lists the scattering and absorption cross sections for the measurement processes of interest. It is readily apparent that absorption and fluorescent cross sections are about ten orders of magnitude larger than

TABLE II

REPRESENTATIVE CROSS SECTIONS

Process	Cross Section $\frac{d\sigma}{d\Omega}$ (cm^2)	Lifetime (sec)	Scatterer	Spectral Range (μm)
ELASTIC SCATTERING				
Rayleigh	10^{-27}		N_2 , O_2	$0.20 \approx 1.0$
Mie	$10^{-21} - 10^{-24}$		particulates, aerosols	$0.20 \approx 10$
INELASTIC SCATTERING				
Raman	10^{-30}		all molecules	uv, visible
Resonance fluorescence and Fluorescence				
uv, visible	$10^{-14} - 10^{-17}$	$10^{-6} - 10^{-8}$	atoms,molecules	uv, visible
IR	$10^{-18} - 10^{-23}$	$10^{-1} - 10^{-6}$	molecules	2 - 20
ABSORPTION				
uv, visible	$10^{-14} - 10^{-17}$		atoms, molecules	uv, visible
IR	$10^{-17} - 10^{-21}$		molecules	2 - 20

Raman scattering cross sections. This physical fact leads to the immediate conclusion that the most sensitive remote detection methods are by absorption. Resonance fluorescence and fluorescence also have cross sections that are nearly that of absorption. However, for monitoring in the troposphere quenching reduces the fluorescence cross section. Quenching is not a problem at high altitudes and remote monitoring by resonance fluorescence has a clear advantage in that case.

We can now return to Eq. (8) and consider the effective reflectivity of the "target" for remote sensing. Table III lists the scattering process and the corresponding effective reflectivity.

For absorption measurements with a remote sensor or retroreflector and a collimated transmitted beam, the range squared dependence is effectively cancelled. Thus all of the transmitted power is collected except for a collection efficiency factor ξ, which is near unity, and the effective target reflectivity is orders of magnitude better than for a Lambertian scatterer. Letting $\rho/\pi = R^2\xi/A$ in Eq. (8) reduces it to the form commonly used to describe long path absorption.

For long path absorption by scattering from topographic targets, $\rho \approx 1$ for all infrared wavelengths and $\rho \sim .1$ for ultraviolet and visible wavelengths.[55] Thus the effective target reflectivity is approximately $1/\pi$. For single ended long path absorption measurements from topographic targets over kilometer ranges, 10^4 - 10^6 more transmitted power is required than for doubled ended measurements using a remote detector or retroreflector. Since the required power for double ended long path absorption is less than one microwatt,[1] single ended measurements can be made with milliwatt to watt laser sources. The HeNe laser geodolite ranging systems are an example of single ended range

TABLE III

EFFECTIVE REFLECTIVITY

Method	(ρ/π)	Magnitude
Long Path Absorption with Retroreflector	$\frac{R^2\varepsilon}{A}$	$10^4 - 10^6$
Long Path Absorption from Topographic Target	ρ/π	$1/\pi$
Differential Absorption	$\left(\frac{c\tau}{2}\right)\frac{\beta_{Mie}}{4\pi}$	10^{-4}
Resonance Fluorescence and Fluorescence	$\left(\frac{c\tau}{2}\right)\frac{N\sigma_F}{4\pi}$	10^{-5} (1 ppm) (uv and visible)
Raman	$\left(\frac{c\tau}{2}\right)\frac{N\sigma_{RAM}}{4\pi}$	10^{-15} (1 ppm) 10^{-9} (1 atm)

measurements by scattering from topographic targets.[61]

Remote detection by backscattering involves the range resolution $\Delta R = \frac{c\tau}{2}$ as well as the backscattering cross section. For Mie backscattering the returned power is independent of the pollutant concentration and depends only on the Mie backscatter coefficient β_{Mie}. For resonance fluorescence and Raman backscattering, the returned signal depends on the scattering cross section and on the pollutant density. The dependence on pollutant density reduces the returned signal for weak pollutant concentrations and thus also reduces the measurement S/N ratio which further effects the detection sensitivity. For depth resolved pollutant measurements differential absorption has the advantages of a relatively large effective reflectivity which is independent of pollutant concentration and the additional advantage of the large absorption cross section which is not affected by quenching.

To complete the general formulation of remote pollutant detection we need to introduce detector parameters and evaluate the detector S/N ratio for a given returned power. This procedure has been discussed previously,[1,4,5,33] but a summary is useful here.

The voltage signal to noise ratio for a detector is

$$\frac{S}{N} = P_r / \left[4P_r\left(\frac{h\nu}{\eta}\right)\Delta f + 2\,NEP^2\,\Delta f\right]^{\frac{1}{2}} \qquad (10)$$

where P_r is the received signal power and Δf is the amplifier bandwidth. The first term in the denominator is due to the shot noise generated by the signal itself. Here $h\nu$ is the photon energy and η is the detector quantum efficiency. The second term in the denominator represents the noise of the

detector in the absence of the signal (dark current and background noise and preemplifier noise characterized by the noise equivalent power NEP). A factor of 2, added under the square root, takes account of the noise resulting from two measurements required to determine the pollutant concentration. This noise is $P_N^2 = (P_N^2)_{on} + (P_N^2)_{off}$ where on and off refer to making the measurement on resonance and off resonance of the characteristic line of the pollutant. Usually either the first or the second term in the demoninator need to be considered.

For shot noise limited detection the dark current term in the denominator can be neglected. For practical purposes this limit can be attained with photomultipliers if all background radiation is adequately filtered. At a given signal to noise ratio, the minimum detectable power from Eq. 10 is given by

$$P_r^{min}(\text{shot noise}) \geq 4\left(\frac{h\nu}{\eta}\right) F \left(\frac{S}{N}\right)^2 \Delta f \qquad (11)$$

where the factor F has been added (between 2 and 5) to account for the partition noise effect of the multiplier dynodes. Equation (11) gives the minimum detectable power for current measurements.

Photomultipliers can also be used in the photon counting mode. For count rates greater than approximately 10^3 sec^{-1} the photon counting method and current detection method give equal sensitivities. However, for low count rates photon counting offers an improvement in signal to noise ratic by the factor F . Thus for weak signals photon counting is preferred while for more intense signals and wide dynamic range the boxcar integration technique is more useful.[4]

An important extension of the shot noise detection regime is heterodyne detection. The nonlinear response of the photo-detector allows the generation of a mixing frequency at the intermodulation frequency of the two applied light

fields. The heterodyne signal to noise ratio for detection at the IF frequency is[62]

$$P_r^{min}(\text{heterodyne}) \geq \frac{2\,h\nu\left(\frac{S}{N}\right)^2 \Delta f}{\eta} \quad \text{(photoemitter reversed biased diode)} \tag{12a}$$

$$\geq \frac{4h\nu\left(\frac{S}{N}\right)^2 \Delta f}{\eta} \quad \text{(photoconductor photovoltaic diode)} \tag{12b}$$

where the extra factor of 2 for the photoconductor detector is due to generation-recombination noise.

The required local oscillator power is such that the shot noise term in the denominator of Eq. (10) equals the dark current or amplifier NEP term. This condition can be written in a number of ways depending on the expressions for the NEP.[63] However, if amplifier noise dominates and is expressed as an equivalent noise temperature T_A then

$$P_{LO} = \frac{(k\,T_A)\,h\nu}{\eta\, e^2 G^2 R_L} \tag{13}$$

where e is the electron charge, G the detector gain and R_L the load resistance.[64] For example, for an amplifier with noise temperature of 240 K (noise figure 2.4 dB) and assuming $\eta = 0.5$, $G = 0.12$, $R_L = 50\ \Omega$ and $\lambda = 10\ \mu m$ we obtain $P_{LO} = 12$ mW. This is a rather high local oscillator power since it may result in detection heating. However, wide band photodiode detectors with unit quantum efficiency should require much less ($\sim$100 μ W) local oscillator power to reach the quantum limit.

Heterodyne detection offers extreme spatial filtering due to its antenna like properties and the short optical wavelength involved. Siegman[66] has shown that the effective aperture of a heterodyne detector is $A_R \Omega_R \simeq \lambda^2$ where A_R is the effective receiver aperture and Ω_R the receiver solid angle. Thus in addition to orders of magnitude more sensitivity than dark current limited detection, the heterodyne detector offers diffraction limited spatial filtering against the incident background radiation.

A potentially useful form of heterodyne detection for remote monitoring is infrared up-conversion in a nonlinear crystal. The noise power for an up-efficiency ε onto a shot noise limited photomultiplier is [67]

$$P_r^{min}(\text{up-conversion}) = \frac{4 h\nu \left(\frac{S}{N}\right)^2 \Delta f}{\eta \varepsilon} \qquad (14)$$

which is equivalent to the previous expression for heterodyne detection by a photoconductor. Using a cw argon ion laser at 1W power to pump a $LiNbO_3$ crystal Smith and Mahr[68] were able to up-convert and detect 3 μm radiation at a NEP of 10^{-14} W. Up-conversion offers wider acceptance bandwidth (~100 GHz) compared to heterodyne mixing detection (~1GHz) and yet still maintains spatial and spectral filtering.

The useful properties of heterodyne detection has led to the suggestion of remote detection of pollutants by monitoring thermal induced fluorescence from hot effluent gases.[3,64,65] Menzies[69,70] has evaluated the use of heterodyne detection for remote monitoring and has recently[31] demonstrated room temperature detection of ozone, sulfer dioxide, ammonia and ethylene using a CO_2 laser as a local oscillator.

Heterodyne techniques can also be applied to improve the detection capabilities of any remote monitoring method. However, the cost and complications of present tunable coherent sources has prevented the wide application of heterodyne detection.

For dark current or background limited detection the minimum detectable power evaluated from Eq. (10) is

$$P_r^{min}(\text{dark current}) = \text{NEP}\left(\frac{S}{N}\right)\sqrt{2\Delta f} \quad . \qquad (15)$$

This type of detector noise limitation applies, in particular, to photoconductors and other detectors used in the infrared. It is characteristic for dark current limited detectors that they achieve, for constant average power, a higher signal-to-noise ratio with increasing peak power in pulsed operation.[71]

Detector performance is also expressed in terms of the detectivity D^* which is related to the NEP by $D^* = \sqrt{A}/\text{NEP}$ where A is the detector area. Typical values of D^* are 6×10^{12} cm $Hz^{\frac{1}{2}}/W$ for room temperature silicon diodes, 3×10^{11} cm $Hz^{\frac{1}{2}}/W$ for $77^{\circ}K$ operation of InAs (1 μm - 3.3 μm) photovoltaic detectors, 1.1×10^{11} cm $Hz^{\frac{1}{2}}/W$ for $77^{\circ}K$ InSb (1.5 μm - 5.5 μm) photovoltaic detectors,to 2×10^{10} cm $Hz^{\frac{1}{2}}/W$ for $77^{\circ}K$ HgCdTe(2 μm to 25 μm) detectors. The rise time of these detectors is less than 100 nsec. Finally, detector costs vary from approximately $100 for silicon diodes to $1,000 for recently developed HgCdTe detectors. A complete manufacturers reference to detectors is given in a recent trade journal issue.[72]

In the above expressions for detector minimum detectable power, we have assumed Δf is the electronic bandwidth required to resolve a pulse. More

specifically we take $\Delta f\tau = 2$ as the condition necessary to resolve a pulse of width τ. For pulsed generation the effective detector bandwidth decreases with the number of averaged pulses n as $\Delta f/n$.

We are now in a position to combine Eq. (8) for the received power with the expressions for minimum detectable power and solve for the detection parameter of interest at specified values of the other variables. The parameters of interest are required transmitted energy vs range, S/N ratio vs range at a fixed energy, and minimum detectable pollutant concentration relative to one atmosphere, η, at a given transmitted energy and range. The above procedure is carried out and the results are discussed for Raman scattering, fluorescence backscattering, the integrated path absorption methods, and for the differential absorption method in the following sections.

B. Raman Method

Remote atmospheric monitoring by Raman backscattering was first demonstrated in 1967 by Leonard.[20] The early work in Raman scattering including the detection of water vapor[21,22,25] and SO_2 and CO_2[24] was discussed in the introduction.

Early remote pollutant detection work was limited to Raman scattering because of the lack of high peak power tunable laser sources. The principle advantage of the Raman method is the use of a fixed frequency laser transmitter. The other apparent advantages include operation in the visible or ultraviolet and the use of photomultiplier detectors and the detection of homo-nuclear molecules N_2 and O_2 in addition to other molecules of interest. On the other hand, the disadvantages of remote detection by Raman scattering include very small Raman scattering cross sections and therefore lack of sensitivity, operation in the visible with high energy laser sources and the resultant eye safety problem,

and simultaneous excitation of the Raman scattering of all molecules present thus requiring a spectrometer filter to adequately isolate the Raman signal of interest. Of these disadvantages, it is the lack of sensitivity that has forced thinking about improvements of the Raman method and the remote detection of pollutants by other methods.

An interesting benefit of the remote Raman detection work has been the measurement of absolute Raman cross sections of gases. Inaba and Kobaysi[4] provide a table of measured Raman cross sections in their review paper. However, additional measurements are still being made[73] as evidenced by a very recent absolute Raman cross section measurement of N_2.[74]

To evaluate the sensitivity and required transmitted energy for the Raman method we substitute the expression for the minimum detectable power for a shot noise limited photomultiplier given by Eq. (11) into Eq. (8) and replace (ρ/π) in Eq. (8) by $\frac{N\sigma_{RAM}}{4\pi}\left(\frac{c\tau}{2}\right)$ as given in Table III. Solving for the transmitted power we find

$$P_0 = \frac{1}{K}\left[4\left(\frac{h\nu}{\eta}\right) F \left(\frac{S}{N}\right)^2 \Delta f\right] \frac{4\pi}{N\sigma_{RAM}} \frac{2}{\tau c} \frac{R^2}{A} \exp\left[2\int_0^R \alpha_A(r)\, dr\right] \qquad (16)$$

where the terms in the brackets give the detector minimum detectable power P_r^{min} for a shot noise limited detector. For shot noise limited detection the highest average power is of interest. However, for depth resolution and to remain in the shot noise limited detection range, pulsed laser sources are usually used. Multiplying Eq. (16) by τ, the required transmitted energy of pulse width τ is given by

$$E_0 = P_0 \tau = \frac{1}{K}\left[4\left(\frac{h\nu}{\eta}\right) F \left(\frac{S}{N}\right)^2 \Delta f \tau\right] \frac{4\pi}{N\sigma_{RAM}} \frac{1}{\Delta R} \frac{R^2}{A} \exp\left[2\cdot\int_0^R \alpha_A(r)\, dr\right] \qquad (17)$$

As an example, we consider the Raman detection of CO at 0.347 μm, the doubled Ruby laser output wavelength. At this wavelength $(d\sigma/d\Omega)_{CO} = 3.6 \times 10^{-30}$ cm^2.[4] We let the atmospheric volume extinction coefficient be a constant 1 km^{-1} corresponding to a visibility of approximately 5 km, and assume a photomultiplier detector with F = 4 and a 20 MHz bandwidth required to resolve a 100 nsec pulse. For a 1J, 100 nsec transmitted pulse and a 1000 cm^2 area receiving telescope at K = .1 we find the minimum detectable pollutant concentration vs range shown in Fig. 2. Also shown in Fig. 2 are the peak and average CO levels for urban atmospheres.

It is readily apparent that the Raman method does not have the sensitivity required for ambient pollutant concentration measurements. However, the Raman method does have adequate sensitivity to monitor N_2, O_2 and H_2O to a few kilometer range.

Using a nitrogen laser operating at 3371 Å at 20 kW peak power 10 ns half-width at 50 pps, Kobayasi and Inaba[75] have detected Raman signals from clear air and from an oil smoke plume. The receiving system consisted of a 30 cm diameter telescope followed by an f 8.5 half meter grating monochromator and spectral interference filter. The signal was detected by a photomultiplier and boxcar integrator sampling circuitry and displayed on an X-Y recorder. Figure 3a shows the return from ordinary air at 30 m range. The N_2 and O_2, O and S as well as Q branches are evident. Also evident is the strong Rayleigh and Mie backscattered signal which must be suppressed for Raman measurements but which is very useful in the differential absorption method considered later.

Figure 3b illustrates the Raman return from oil smoke. Here the N_2 and O_2 peaks provide a calibration for the other molecular return signals of interest.

However, the spectral width and intensity of the O and S branches tend to interfer with the Raman signal of the more weakly concentrated smoke plume constituents. Also indicated is the fluorescence return which may be a useful signal for some remote monitoring applications discussed in the following section.

The use of a photomultiplier detector, and the intense Rayleigh and Mie backscattered signal compared to the Raman signal presents significant filtering problems against background signal. The requirements for background filtering were discussed by Kildal and Byer[1] who showed that the background signal must be less than the Raman signal if sensitivity is to be maintained. This requirement forces the consideration of grating monochromators and interference spike filters in the receiving system thus adding complications and lowering its optical efficiency. Recently, Cooney[76] proposed a differential Raman measurement using N_2 and O_2 as a reference to eliminate the common background and allow daytime operation.

Progress in laser sources has led to improvement in Raman detection systems. For example Hirschfeld et al.,[77] describe a frequency doubled Ruby laser transmitter with a 3 m receiving aperture telescope system which has been used in the field to detect CO_2, H_2O and SO_2 over a 200 m range. The 2J, 2pps Ruby laser source was doubled in KDP with 8% efficiency and the returned signal was processed by photon counting techniques referenced against the nitrogen signal in a differential manner. Range gating provided a 10 m depth resolution. This Raman detection system probably represents the state of the art for sensitivity and range.[78]

Recently Raman scattering has been used to vertically probe the atmosphere to a height of up to 6 km. The Raman-laser system is described by Kent et al.,[79] and the measurements and probably extension to 40 km height is discussed by Garvey and Kent.[80] The application of Raman scattering return from N_2 for

temperature measurements has been considered by Strauch et al.[26] Experimental results over a 30.5 m range at a 5 m depth resolution confirmed the Raman backscatter vs temperature correlation and indicated a differential temperature sensitivity near 3°.

Despite the above success of the Raman method, its lack of sensitivity has severely limited its application to ambient pollutant monitoring. A number of suggestions have been made to improve the Raman sensitivity. They include using resonance to enhance the Raman cross section, using interferometric methods to improve receiver entendue and applying four wave Raman mixing to generate a coherent anti-Stokes signal with high efficiency.

Resonance Raman scattering has achieved considerable recent attention due to the potential of improving the Raman cross section by tuning the probing laser radiation near an electronic resonance. The general form of the third order susceptibility in Eq. (5) is[81]

$$\chi^{(3)} \alpha \frac{1}{(\omega_1 - \omega_a)(\omega_1 - \omega_2 - \omega_R + i\,\Gamma_R)(2\omega_1 - \omega_2 - \omega_b)} \qquad (18)$$

where ω_a and ω_b are electronic frequencies and ω_R is the Raman frequency. As ω_1, the exciting frequency, approaches an electronic resonance ω_a, $\chi^{(3)}$ is resonantly enhanced. The enhanced Raman cross section still falls well short of the on resonance fluorescence cross section.[1,82] Experimental work has verified the theory for both atoms[83] and molecules.[84-87] For remote detection the tunable laser source required to achieve Raman resonance enhancement is probably better utilized by tuning exactly on resonance and exciting resonance fluorescence. In that case the fluorescence return, even if quenched, is still about two orders of magnitude greater than the resonance Raman return.[1]

The rotational Raman scattering cross sections are larger than the vibrational-rotational cross sections and interferometric filtering has been proposed to take advantage of this to improve Raman sensitivities.[88] However, the rotational lines of most molecules lie within 100 cm^{-1} of the exciting line and overlap interference is a severe problem. These reasons have prevented realization of the expected improvement in sensitivity.[89]

A novel application of tunable laser sources to Raman detection is coherent anti-Stokes Raman spectroscopy by four wave mixing.[81] In this coherent Raman scattering process, a tunable laser mixes with a pump laser to generate a coherent laser-like anti-Stokes output beam. The Raman susceptibility shows resonance when $\omega_1 - \omega_2 - \omega_R = 0$ according to Eq. (18) where ω_1 is the pump frequency, ω_2 the tunable frequency and ω_R is the Raman resonant frequency of the medium.

The coherent anti-Stokes beam is generated with a conversion efficiency given by[35]

$$\frac{P(\omega_3)}{P(\omega_2)} = \frac{2.77 \times 10^{-3}}{n^4 \lambda_3^2} \left| N \chi''_{RAM} \right|^2 \ell_{coh}^2 I_1^2 \qquad (19)$$

where N is the density, χ''_{RAM} is given by Eq. (5) in terms of $d\sigma_{RAM}/d\Omega$, ℓ_{coh} is the coherence length in cm which in liquids is approximately 0.1 cm but in gases is near 100 cm, and I_1^2 is the pump intensity in W/cm^2. Here $N \chi''_{RAM}$ is the bulk Raman susceptibility in esu units (cm^3/erg) and λ_3 is the anti-Stokes wavelength in cm.

The advantages of four wave Raman mixing are the very high conversion efficiencies to the anti-Stokes frequency, the spatially coherent output beam, and the discrimination against background fluorescence. These advantages have

been experimentally verified in liquids where up to 1% conversion efficiencies have been observed in benzene.[90]

Four wave Raman mixing has also been used to measure small gas concentrations by Regnier and Taran.[91] They used a Ruby laser pumped stimulated molecular hydrogen Raman source mixing with the remaining Ruby light to measure H_2 concentrations down to 100 ppm in nitrogen. Below 100 ppm the background third order susceptibility of N_2 gave rise to a signal which interfered with the weak H_2 anti-Stokes signal. With presently available high peak power tunable laser sources four wave Raman mixing should provide a valuable technique for the investigation of gases down to the ppm level. Although the input beams must be focused in the medium, the spatially coherent output beam can be remotely monitored thus providing a local pollutant monitoring system with a probe that is completely free from the volume of interest. Recent work has verified the important parameters of four wave Raman mixing in liquids and gases, but more research is necessary to evaluate the remote detection possibilities.

C. Resonance and Fluorescence Scattering

In 1969 Bowman et al.,[92] used a tuned dye laser to detect sodium in the upper atmosphere by resonance backscattering. By 1970 regular measurements[93,94] were being made of the sodium double layer at 90 km altitude. Since that time observations of the sodium layer have been numerous[95-98] and recently they have been extended to daytime[99] and to potassium.[100]

The use of resonance and fluorescence backscattering for probing the troposphere has been limited. However, the method has been extensively analyzed by Kildal and Byer[1] and recently by C.M. Penney et al.,[101] Resonance backscattering has also been discussed by Kobaysi and Inaba[75] and by Measures and Pilon.[5]

To evaluate the returned signal power due to resonance and fluorescence backscattering we proceed as before for the Raman method. However, we must now consider the additional complication of a finite fluorescence lifetime which both reduces the returned power and smears out the depth resolution. An exact analysis of the returned power for a finite fluorescence lifetime was given by Kildal and Byer[1] and is summarized here.

In general, the returned signal power is given by

$$P_r(R) = KE_o \frac{N\sigma_F}{4\pi} \frac{1}{\tau_{sp}} \left(\frac{\omega_F}{\omega_T}\right) A \frac{S(t)}{R_{min}} \tag{20}$$

where ω_F and ω_T are the fluorescence and transmitted frequencies, σ_F is the fluorescence cross section without quenching , R_{min} is the range to the beginning of the pollutant cloud. $S(t)$ is a dimensionless integral with a peak value of unity given by

$$S(t) = R_{min} \frac{\tau_F}{\tau_p} \left\{ \int_{c(t-\tau_p)/2}^{c\tau_F/2} \frac{dR}{R^2} \left(1 - \exp\left[-\frac{1}{\tau_F}\left(t - \frac{2R}{c}\right)\right]\right) \right.$$

$$\cdot \exp\left[-\sigma_F N(R - R_{min})\right] + \left[1 - \exp(-\tau_p/\tau_F)\right] \int_{R_{min}}^{c(t-\tau_p)/2} \frac{dR}{R^2} \cdot$$

$$\left. \cdot \exp\left[-\frac{1}{\tau_F}\left(t - \tau_p - \frac{2R}{c}\right) - \sigma N(R - R_{min})\right] \right\} \tag{21}$$

where τ_F is the radiation decay time which is less than τ_{sp}, the spontaneous decay time, due to quenching and τ_p is the laser pulse width. The integral $S(t)$ has been studied in detail and it is plotted vs time for a number of cases of interest.[1] In general it reflects the increased time over which fluorescence returns to the detector due to the finite radiation decay time of the fluorescence. The fluorescence decay time leads to a depth resolution given by Eq. (9) in which τ_F is the dominant term. For infrared transitions the depth resolution varies between .15 km and 15 km thus preventing depth resolved measurements. For visible and ultraviolet transitions, quenching reduces the radiative lifetime to the order of nanoseconds so that the depth resolution equals that for Raman scattering.

For visible and ultraviolet transitions, the integral $S(t)$ simplifies to

$$S(t = \frac{2R}{c}) \approx R_{min} \frac{c\tau_F}{2} \frac{\exp[-\sigma_F N(R - R_{min})]}{R(R - c\tau_p/2)} .$$

If we let $R \gg c\tau_p/2$ which is the usual case of interest, then $S(t)$ reduces further to

$$S\begin{pmatrix}\text{visible}\\ \text{ultraviolet}\end{pmatrix} \approx R_{min} \frac{c\tau_F}{2R^2} \exp\left[-2 \int_0^R \alpha_A(r)dr\right] \qquad (22)$$

where we have incorporated the pump depletion due to absorption by the fluorescing species $\exp -\sigma_F N(R - R_{min})$ into the total atmospheric extinction term

$$\exp\left[-2 \int_0^R \alpha_A(r)dr\right] .$$

Substituting Eq. (22) into Eq. (20) gives for the power received at the detector due to backscattered fluorescence

$$P_r(R) = KE_o \frac{N\sigma_F}{4\pi} \cdot \frac{\tau_F}{\tau_{sp}} \cdot \frac{c}{2} \frac{\omega_F}{\omega_T} \cdot \frac{A}{R^2} \exp\left[-2 \int_0^R \alpha_A(r)dr\right] . \quad (23)$$

If we note that $\sigma_{ABS} = \sigma_F/Q$ where Q is the Stern-Volmer quenching factor[102]

$$Q = \frac{1}{1 + \frac{\tau_{sp}}{\tau_{col}}\left(\frac{1}{Z}\right)} \approx \frac{\tau_{col}}{\tau_{sp}} Z$$

with $1/Z$ the probability of quenching per collision and τ_{col} the collision time which is approximately 10^{-10} sec at atmospheric pressure, then Eq. (23) can be written in a form identical to that for Raman scattering except that σ_{RAM} is replaced by $\sigma_{ABS}\, Q$. Thus

$$P_r(R) = KP_o \frac{N\sigma_{ABS}}{4\pi} Q \cdot \frac{c\tau}{2} \frac{\omega_F}{\omega_T} \frac{A}{R^2} \exp\left[-2 \int_0^R \alpha_A(r)dr\right] \quad (24)$$

where the effective reflectivity $\left(\frac{\rho}{\pi}\right)$ equals $\left(\frac{c\tau}{2}\right) \frac{N\sigma_{ABS}Q}{4\pi}$ for quenched backscattering in agreement with Table III.

The two cases of interest in evaluating fluorescence backscatter are infrared backscatter from molecular vibrational-rotational transitions and visible or ultraviolet resonance and fluorescence backscatter from atoms and electronic transitions of molecules. Fluorescence cross sections and quenching factors have been listed and are not repeated here.[1,75]

For the infrared case the power received at the detector given by Eq. (20) is equated to the minimum detectable power for a dark current limited detector given by Eq. (15) and the minimum pollution concentration is found as a function of transmitted energy and range at a given set of parameters. In this case, only a fraction, f , of the total fluorescence band is monitored, for example, a single vibrational-rotational line. The integral S(t) cannot be simplified and must be evaluated. Figure 4 shows the result of an evaluation for CO at 4.6 μm assuming an InSb detector, a 100 mJ transmitted pulse and a S/N = 1 . The other parameters of interest are given in the figure. The integral S(t) evaluates differently for thin and thick pollutant layers. For a thin layer the pump depletion due to absorption by the pollutant is negligible while for a thick layer the transmitted pump beam is totally depleted within the layer. Optically thick pollutant layers prevent depth resolved measurements due to transmitted pump depletion over a length $\Delta R_{depl} \sim 1/(\sigma_{ABS} N)$. The large atomic and molecular electronic cross sections make optically thick pollutant clouds a distinct possibility in the visible and ultraviolet. Measures and Pilon[5] present calculations showing the resonance detection of optically thick layers and the resultant pump depletion and loss of depth resolution.

For the visible and ultraviolet case the power backscattered to the detector is given by Eq. (24). Equating the received power to the shot noise limited minimum detectable power given by Eq. (11) gives for the required transmitted energy

$$E_o = \frac{1}{fK}\left[4\left(\frac{h\nu}{\eta}\right) F \left(\frac{S}{N}\right)^2 \Delta f \tau\right] \frac{4\pi}{N\sigma_{ABS} Q} \frac{1}{\Delta R} \frac{R^2}{A} \exp\left[2 \int_0^R \alpha_A(r) dr\right] \quad (25)$$

where f is the fraction of total fluorescence monitored, $\Delta R = c\tau/2$ is the range resolution and the other quantities have been previously defined.

Equation (25) is similar to the previously derived result for Raman scattering given by Eq. (17), except that the required transmitted energy is reduced from the Raman case by the ratio $\sigma_{RAM}/f\sigma_{ABS}Q$ which is approximately 10^{-2} for molecular pollutants and 10^{-8} - 10^{-10} for atomic pollutants such as sodium and mercury. Examples of detection sensitivities for electronic molecular transitions and atomic transitions are given by Kildal and Byer,[1] Kobaysi and Inaba[75] and by Measures and Pilon.[5]

Recently Gelbachs et al.,[103] utilized resonance fluorescence of NO_2 excited by an argon ion laser to detect NO_2 locally with a sensitivity of one part per billion. The laser excitation was at .488 μm and the fluorescence was monitored at 0.7 to 0.8 μm . Local Los Angeles air, drawn through filters, was monitored and NO_2 variations measured over a few hour period showed peak concentrations near 0.1 ppm on smoggy days and 0.03 ppm on smog free days. Filtering the air was necessary to eliminate interfering fluorescence from particulates in the air.

The increased sensitivity of resonance and fluorescence backscattering makes it appear useful as a remote monitoring method compared to the Raman method. However, the requirement for a tunable laser, the lack of depth resolution in the infrared, and the not precisely known fluorescence cross section due to the unknown local quenching factor, severely limit the usefullness of resonant backscatter or fluorescent backscatter as a remote pollutant measurement method in the troposphere. Finally, as will be shown later, the sensitivity of the fluorescent backscatter method is surpassed by that of the differential absorption method which does not suffer from quenching or return signal strength dependence on pollutant density or cross section.

An alternate approach to monitoring radiated fluorescence is to apply the tunable coherent radiation to the detector to increase its sensitivity by heterodyne detection. Heterodyne detection was discussed in Section IIA so here only an estimate of detection sensitivity is considered.

The sky brightness in watts $m^{-2}Hz^{-1}rad^{-2}$ due to thermal radiation with emissivity ϵ_b for a single polarization is

$$B = (h\nu^3/c^2)\left(\frac{1}{\exp h\nu/kT_B - 1}\right) \qquad (26)$$

The power received at the heterodyne detector is given by Eq. (7) with $\Delta\lambda$ replaced by the I.F. bandwidth, B , and $\Omega_m A_m = \lambda^2$ for heterodyne detection[66] so that

$$P_r^{off} = \frac{\epsilon_g h\nu B}{\exp(h\nu/kT_B) - 1} \qquad (27)$$

where ϵ_B is the background atmospheric emissivity.

The signal received from a pollutant cloud filling the field of view at temperature T_p is

$$P_r^{on} = \frac{[1 - \exp(-N\sigma_{ABS}L)]}{\exp(h\nu/kT_p) - 1} h\nu B \qquad (28)$$

where the emissivity of the pollutant gas is related to the absorptivity by Kirchoff's law. The signal to noise for heterodyne detection of an emitting pollutant cloud is found by setting $(P_r^{on} - P_r^{off})$ equal to the heterodyne minimum detectable power given by Eq. (12b). The resulting voltage signal to noise ratio squared is

$$\left(\frac{S}{N}\right)^2 = \frac{\eta}{4}\left[\frac{1 - \exp(-N\sigma_{ABS}L)}{\exp(h\nu/kT_p) - 1} - \frac{\epsilon_B}{\exp(h\nu/kT_B) - 1}\right] B\tau \qquad (29)$$

where $\tau = 1/\Delta f$ is the integration time. Since the emissivity of the background is usually less than 1, the temperature of the pollutant gas can be less than the surrounding air and still be detected.

Figure 5a and 5b show the sensitivity limits of heterodyne detection of SO_2 and CO_2 vs the IF bandwidth-integration time product. The detectable concentration is given as an equivalent absorption coefficient where 10^{-2} atm cm is equivalent to 1 ppm km. Figure 5a shows the sensitivity limits calculated by Menzies[70] for SO_2 with a measured absorption coefficient of 0.58 atm^{-1} cm^{-1} at room temperature using a $C^{12}O_2^{18}$ laser as the local oscillator. Figure 5b shows the calculated CO_2 detection sensitivity at $T = 450^{\circ}K$ for all the mixing signal falling on the detector (solid line) and for 20% falling on the detector which corresponded to the experimental condition. The crosses indicate actual measured sensitivities.

These results show that heterodyne detection is useful for remote monitoring of hot effluent gases from concentrated sources. However, the sensitivity of the heterodyne method is still not adequate for dispersed pollutant measurement and is not nearly as sensitive as absorption methods to be discussed in the following section.

D. Long Path Absorption Methods

Long path absorption for the detection of atmospheric pollutants using laser sources is an extension of well known methods.[104,105] However, the laser source with its spatial collimation, very high spectral resolution and high power offer significant advantages over previously used incoherent sources. Closed path double ended long path absorption and open path single ended long path absorption using topographical targets are discussed in this section. These measurement methods provide the most sensitivity at the least required transmitted power of any of the remote detection methods.

Remote air pollutant detection using laser sources was discussed as early as 1967 by Jacobs and Snowman.[106] Later Hanst[28,107] described pollutant detection using fixed frequency laser coincidences with absorbing lines. More recently, Zaromb,[108] and Japanese workers[109,110] described remote sensing by laser absorption and Hodgeson et al.,[111] considered advanced monitoring techniques. Kildal and Byer[1] have given a detailed analysis of the doubled ended long path absorption method. The analysis was later extended to the single ended absorption method using topographical targets by Byer and Garbuny.[33]

Double ended long path absorption experiments have been carried out using low power diode lasers[112] by Hinkley[3,65] and using CO_2 lasers by Snowman.[113] Recently an argon ion laser has been used to detect NO_2.[114] The topographical single ended absorption method was first demonstrated by Henningsen et al.,[115] in the infrared using a parametric tunable laser source. The parameters of importance for long path absorption measurements and the detection sensitivity are discussed in this section along with recent experimental results.

The long path resonance absorption method measures the total integrated pollutant concentration over the path. It has the advantages of increasing sensitivity with range, the largest interaction cross section which is not modified by quenching, and the least required transmitted laser power. It has the disadvantages of being double ended and of lacking depth resolution.

The transmitted intensity at the detector follows from Eq. (8) if we let $(\rho/\pi) = R^2/A$, assume a round trip, and separate the beam attenuation due to pollutant absorption from the atmospheric attenuation. We then have

$$P_r^{on}(R) = KP_o \exp\left[-2\int_0^R \sigma_{ABS} N(R')\, dR'\right] \cdot \exp\left[-2\int_0^R \alpha_A(R')\, dR'\right] \qquad (30)$$

where $N(R')$ is the pollutant density over the range R and we assume that the transmitted intensity is less than the absorption saturation intensity.

The returned power for the pump frequency tuned off the absorbing transition is

$$P_r^{off} = KP_o \exp\left[-2\int_0^R \alpha_A(R')\, dR'\right] \qquad (31)$$

so that the integrated pollutant concentration is determined by the log ratio of the on and off returned power as

$$2\int_0^R N(R')dR' = \frac{1}{\sigma_{ABS}} \ell n \left(\frac{P_r^{off}}{P_r^{on}}\right) \cdot \qquad (32)$$

Assuming that it is possible to measure a 1% change in transmitted power when tuned on and off the absorbing line, the minimum integrated density is given by

$$\left[2\int_0^R N(R')\, dr\right]_{min} = \frac{0.01}{\sigma_{ABS}} \cdot \qquad (33)$$

Table IV lists representative absorption cross sections for molecules and atoms and gives the minimum detectable pollutant concentration for an absorption length R of 100 meters. Since the absorption cross sections are the largest of the Raman, resonance or fluorescence cross sections these sensitivity limits are the best obtainable by optical means. Thus there is a physical limitation for pollutant detection that leads to a depth resolution-sensitivity trade off. Fortunately, σ_{ABS} is large enough that an absorption distance of 100 m allows ambient pollutant levels to be measured to less than 20 ppb.

The absorption sensitivity can be improved by measuring less than a 1% signal power change. The allowed measurement accuracy is discussed by Kildal and Byer[1] and by Byer and Garbuny.[33] These authors show that to detect a 0.1% change in intensity with an InSb detector requires only 10^{-7} watts of incident power at the detector. There is an optimum value of absorption cross section given by $\sigma_{opt} N = 2.22$ and $\sigma_{opt} N = 1.11$ for shot noise and dark current limited detection. In addition, the signal to noise ratio required to achieve a measurement accuracy $\Delta x/x$ is

$$S/N = \Delta x/x \qquad (34)$$

where $x = 2 N\sigma_{ABS} R$.

Other parameters which affect the measurement accuracy and limit the detection sensitivity are atmospheric turbulence and laser power fluctuations. For cw measurements the atmospheric turbulence is a significant limitation for chopping rates on an off resonance of less than 200 cps. Since the signal to noise ratio improves with higher peak power for dark current limited detectors, the use of Q-switched or pulsed laser sources is advantageous. The laser power

TABLE IV

Minimum Measurable Concentration for an Absorption Length of 100 Meters

	CO	NO_2	SO_2	C_6H_6	Na	Hg
$\lambda(\mu m)$	4.7	.4	.29	.29	.5896	.2537
$\sigma^{abs}[cm^{2*}]$	1.8×10^{-18}	2.8×10^{-19}	3.4×10^{-19}	1.3×10^{-18}	4.8×10^{-13}	5.6×10^{-14}
$\eta(1\%)$	2.1×10^{-8}	1.3×10^{-7}	1.1×10^{-7}	1.5×10^{-8}	7.9×10^{-14}	6.7×10^{-14}

fluctuations can be reduced by careful engineering or by ratio normalization of each laser pulse. The ultimate accuracy achieved by these steps is determined by the dynamic range and linearity of the detector. However 0.1% ratio accuracy is routinely achieved.

The required transmitted power at a given signal to noise ratio for measurement of a pollutant concentration has been shown to be[33]

$$\left.\begin{aligned} \left(\frac{S}{N}\right) &= x\left(P_r^{off}/P_N\right)^{\frac{1}{2}} \quad \text{(shot noise)} \\ \left(\frac{S}{N}\right) &= x\left(P_r^{off}/P_N\right) \quad \text{(dark current)} \end{aligned}\right\} x < 1$$

$$\left.\begin{aligned} \frac{S}{N} &= \left(P_r^{off}/P_N\right)^{\frac{1}{2}} \quad \text{(shot noise)} \\ \frac{S}{N} &= .33\left(P_r^{off}/P_N\right) \quad \text{(dark current)} \end{aligned}\right\} x > 1 \qquad (35)$$

where P_N is given by Eq. (11) for the shot noise limited detection and by Eq. (15) for the dark current limited detector with $S/N = 1$.

For molecules x varies between .1 and 1 for $R = 100$ meters at a concentration of 1 ppm. For atoms x varies between 10 and 300 for $R = 100$ meters at a concentration of 1 ppm. Assuming $x > 1$, for the detection of CO at 4.7 μm with an InSb detector, the required transmitted power from Eqs. (31) and (35) is

$$\begin{aligned} P_o &= \frac{3}{K}\left(\frac{S}{N}\right) P_N \exp\left[2\int_0^R \alpha_A(R')\,dR'\right] \\ &= \frac{3}{K}\left(\frac{S}{N}\right) NEP\sqrt{2Af}\ \exp\left[2\int_0^R \alpha_A(R')\,dR'\right] . \end{aligned} \qquad (36)$$

For an NEP = $.3 \times 10^{-11}$ W/Hz$^{\frac{1}{2}}$, K = .1 a bandwidth of 1 MHz , $\frac{S}{N} = 100$ which implies a 1% detection sensitivity, and assuming $\alpha_A \sim 1$ km^{-1} , the required peak transmitted power for a 1 km range is $P_o = 1$ mW in a 2 μsec pulse. This is well within the range of cw and pulsed infrared lasers and diode lasers.[112]

We can invert the above procedure and ask what is the maximum range for a 1 kW peak power laser source. For $\alpha_A = 1$ km^{-1} we find R = 16 km at a $(\frac{S}{N}) = 100$. Beyond that range the signal to noise ratio decreases reaching unity at 20 km.

These examples show the advantages of long path absorption measurements which include low required transmitted power, long ranges and of course good sensitivity. However, in some situations the requirement for a double ended system is not possible to meet. In those cases the single ended topographical absorption technique is an alternative measurement method.
However, if the transmitter is tunable, then it is possible to sample the optical path for absorption from specific pollutant molecules. The measured integrated density is again given by Eq. (33) for a 1% measured intensity change. Table III again gives the detection sensitivities for a 100 m path.

The advantage of absorption measurements using topographical targets is the single ended measurement with the sensitivity of the closed path absorption method. The disadvantage is the requirement for increased transmitted power.

To find the required transmitted energy for absorption using topographical targets we must consider the measurement procedure carefully since pump depletion due to the pollutant itself may be important.[33]

The power received off resonance is given by Eq. (8) with an effective reflectivity (ρ/π), thus

$$P_r^{off} = \left[\left(\frac{\rho}{\pi}\right) K P_o \frac{A}{R^2}\right] \exp - (2 \alpha_{sc} R) \qquad (37)$$

where $\alpha_{sc} = \alpha_R + \alpha_{MIE}$ is the atmospheric extinction coefficient given by Eq. (2) without the absorption term. If we assume that the atmosphere may itself contain the pollutant gas in a normal concentration N_A which is less than the pollutant concentration N_p, then the power received on resonance is given by

$$P_r^{on} = \left[\left(\frac{\rho}{\pi}\right) K P_o \frac{A}{R^2}\right] \exp\left\{-2R\left[\alpha_{sc} + N_A \sigma_{ABS}\right]\right\} \cdot \exp\left[-2 \sigma_{ABS} \int_0^L N_p(R')\, dR'\right] \qquad (38)$$

where L is the extent of the pollutant cloud. The difference in the power received off resonance and on resonance found by combining Eq. (37) and Eq. (38) is

$$P_r^{off} - P_r^{on} = P_r^{off}\left\{1 - \exp\left[-2 N_A R + N_p L\right] \sigma_{ABS}\right\} . \qquad (39)$$

This difference must be measured relative to the power received at the detector but attenuated by the normally present concentration of gas in the atmosphere given by

$$P_r^{off} - P_r^{on}\Big|_{normal} = P_r^{off}\left\{1 - \exp\left[-2 N_A R\right] \sigma_{ABS}\right\} . \qquad (40)$$

A

For a measurement of the pollutant concentration the difference between Eq. (39) and Eq. (40) must equal the noise power given by Eq. (15) at a given signal to noise ratio, or

$$P_r^{off} \exp[-2 N_A R \sigma_{ABS}] \left| 1 - \exp[-2 N_p L \sigma_{ABS}] \right| = P_r^{min}$$

$$= NEP \left(\frac{S}{N}\right) \sqrt{2\Delta f} \qquad (41)$$

Substituting for P_r^{off} from Eq. (37) and solving for the required transmitted power P_o gives

$$P_o = \left[NEP \left(\frac{S}{N}\right) \sqrt{2\Delta f}\right] \left[\frac{\pi R^2}{\rho K A^2}\right] \frac{\exp 2[\alpha_{sc} + N_A \sigma_{ABS}] R}{1 - \exp(-2 N_p L \sigma_{ABS})}$$

Finally multiplying the above result by τ and setting $\Delta f \tau = 2$ yields for the required transmitted pulse energy

$$E_o = \frac{2}{K} \left[NEP \left(\frac{S}{N}\right) \sqrt{\tau}\right] \frac{\pi}{\rho} \frac{R^2}{A} \frac{\exp 2[\alpha_{sc} + N_A \sigma_{ABS}] R}{1 - \exp(-2 N_p L \sigma_{ABS})} \qquad (42)$$

a result first derived by Byer and Garbuny.[33] The required transmitted energy varies as $\sqrt{\tau}$ as expected for a dark current limit detector. It also increases with range due to the Lambertian scattering properties of the topographical reflector with reflectivity ρ into 2π stearadians.

Equation (42) gives the required transmitted energy assuming that the pollutant of interest is also normally present in the atmosphere. The equation simplifies considerably for most pollutants which are normally not present in

the atmosphere. For this case, the term $\exp(2 N_A \sigma_{ABS} R)$ approaches unity. Finally, if the pollutant cloud itself is optically thin, then the denominator of Eq. (42) reduces to $2N_p L \sigma_{ABS}$. In the limit of a very tenuous pollutant cloud the reduced value of $2N_p L \sigma_{ABS}$ leads to a higher required transmitted energy. Thus we expect that there must be an optimum absorption cross section for a given pollutant density and cloud thickness.

Byer and Garbuny have investigated the optimization of σ for the minimum required transmitted energy. Setting $dE_o/d\sigma = 0$ in Eq. (42) leads to

$$\sigma_{min} = \ell n(1 + q)/2 N_p L \qquad (43)$$

where $q = N_p L/N_A R$. If $N_p L << N_A R$, a situation that may hold for CO detection, then $\sigma_{min} = 1/2 N_A R$. In other words at the optimum value of σ, 2R equals the e^{-1} depletion length. For example, CO normally present in the atmosphere at 0.2 ppm concentration, requires at exact resonance $\sigma = \sigma_{MAX}$ a transmitted laser energy 10^3 larger than for $\sigma = \sigma_{MIN}$ for measurement over a 5 km range.

As an example of long path absorption measurement we consider the detection of CO at 4.7 μm using both long path absorption methods. Consider first the required transmitted energy for topographical target scattering given by Eq. (42). We assume an InSb detection with an NEP = $.3 \times 10^{-13}$ W/Hz$^{\frac{1}{2}}$, a 100 nsec pulse, a 5 km visibility, a 1000 cm^2 area receiver and K = .1. For $\rho = 0.5$ and S/N = 1 for a single pulse we find the required energy vs range shown in Fig. 6. Here σ_{MAX} implies tuning exactly on resonance and σ_{MIN} implies tuning off resonance to satisfy Eq. (43). Here we have assumed that the natural CO abundance between 0.15 - 0.5 ppm (winter) and 0.3 to 3.0 ppm (summer)[116]

leads to an absorption of 0.96 km^{-1}. Figure 6 clearly shows the advantage gained by optimizing the absorption cross section. Figure 6 assumes a CO concentration of 20 ppm over a length of 100 m in the path. For this case $N_A R << N_p L$ up to a range of 10 km. Finally, Fig. 6 shows that for transmitted energies of 20 mJ backscattered absorption measurements are possible for ranges up to 10 km. For most cases in urban areas, a 10 km range is more than adequate, and the single ended advantage of the topographical absorption measurement may offset the disadvantage of higher required laser power.

An alternate way to compare the long path absorption measurement methods is to consider the minimum detectable pollutant concentration vs range. Figure 7 shows the result for the detection of SO_2, NO_2, and CO at the transmitted powers indicated. The methods have comparable sensitivities out to a range where the S/N for the topographical detection begins to fall due to lack of returned signal. Here a S/N ratio of 100 is assumed which allows intensity changes to 1% to be measured. The 100 mJ transmitted energy could be in a single pulse or equivalently in 100 averaged pulses of 10 mJ energy each. Figure 7 illustrates the very high sensitivity of the long path absorption methods and indicates the increase in transmitted power necessary to gain the advantage of a single ended absorption measurement.

The long path absorption methods have been confirmed by experimental measurements.[113] Using diode lasers, Hinkley[3,65,117] has measured C_2H_4 in automobile exhaust locally and over a parking lot area with a retroreflector return. Recently a diode laser system has been constructed for the monitoring of SO_2 stack emissions. The operation of diode lasers at temperatures near 77°K promises to extend considerably their applications to remote monitoring by absorption.

The topographical absorption method was recently experimentally demonstrated by Henningsen et al.[115] They used a 20 μJ , 2.1 μm parametric oscillator source to remotely detect CO by topographical backscattering over a 107 m range. Figure 8a shows the CO overtone spectrum taken in the laboratory with the $LiNbO_3$ tunable parametric laser source. Figure 8b shows two rotation lines of CO taken over the 107 m path. The measurement was not made differentially but by a continuous scan over a few minutes time. Even so, atmospheric scintillation did not reduce the signal to noise significantly. The measured CO detection sensitivity, S/N , and range confirmed the theoretical results given by Eq. (42). Of course more extensive experimental studies need to be made, but the work to date has illustrated the usefullness of the long path absorption methods.

E. Differential Absorption

The differential absorption method overcomes the main disadvantage of the long path absorption methods - lack of depth resolution. By monitoring radiation backscattered from distributed Rayleigh and Mie particulate scattering, and tuning the transmitted wavelength on and off an absorption line of the pollutant molecule, depth resolved absorption measurements can be made with a depth resolution $c\tau/2$ as shown in Fig. 1. The differential absorption method thus combines in an optimum way the depth resolution advantages of the Raman method with the very large absorption cross sections and resultant high sensitivity of the absorption methods. In this section the required transmitted energy, the signal to noise ratio and the sensitivity of the differential absorption method is discussed. Finally, recent experimental results are reviewed to illustrate the advantages of this remote pollutant measurement method.

The differential absorption method was first suggested by Schotland in 1964[118] using a searchlight as a light source. The method was recently discussed by Igarashi[119] and first analyzed in detail by Byer and Garbuny[33] and by Measures and Pilon.[5] Wright[120] has also considered the application of differential absorption to pollution monitoring. In this section we follow the approach of Byer and Garbuny and first find the required transmitted energy, the signal to noise ratio and then the sensitivity of the measurement vs range.

Before proceeding with the analysis, it is useful to schematically describe pollutant measurement by the differential absorption method. Figure 9 illustrates the returned backscattered power when the transmitted wavelength is tuned on and off the CO absorbing transition. The assumed transmitter and receiver characteristics are shown in the figure. The range derivative of $\ell n[P_r^{off}/P_r^{on}]$ equals the CO concentration shown at the bottom of the figure. The differential absorption method thus describes a differential in space with the differential tuning on and off the absorption line being understood. Figure 9 illustrates both the depth resolution and the sensitivity of the differential absorption method.

To evaluate the required transmitted energy for a differential absorption measurement we proceed as previously for the topographical absorption method [cf Eqs. (37) - (42)]. However, now the effective target reflectivity (ρ/π) is replaced by $\frac{1}{2}\, c\tau\beta(R)$ with total backscatter coefficient given by

$$\beta(R) = \beta_R(R) + \beta_{MIE}(R) \qquad (44)$$

where β_R and β_{MIE} are given by Eq. (4) and Eq. (6). However in the infrared, caution must be used in applying Eq. (6).[49,50,121]

Table III shows that the effective reflectivity due to distributed particulate backscattering is approximately four orders of magnitude less than that for topographical targets. Thus the depth resolution advantage obtained by the differential absorption method is acquired at an increased required transmitted energy.

Substituting for ρ/π in Eq. (42) we obtain for the required transmitted energy for the differential absorption measurement method

$$E_o = \frac{4}{K}\left[NEP\left(\frac{S}{N}\right)\frac{1}{\sqrt{\tau}}\right]\frac{1}{c\beta(R)}\frac{R^2}{A}\frac{\exp 2[\alpha_{sc} + N_A \sigma_{ABS}] R}{1 - \exp(-2 N_p L \sigma_{ABS})} \quad . \quad (45)$$

The required transmitted energy now varies as $1/\sqrt{\tau}$ instead of $\sqrt{\tau}$ as for the topographical absorption method because of the bandwidth requirement for depth resolved measurements. Using Eq. (6) to find $\beta_{MIE}(R)$ for a visibility of 5 km and assuming the same parameters as previously for the topographical absorption of CO, we find the required transmitted energy shown in Fig. 10. Here σ_{MAX} is the CO cross section on resonance and σ_{MIN} the optimum cross section given by Eq. (43). At a given range, the differential absorption method requires about three orders of magnitude more transmitted energy than the topographical absorption method. A 10 mJ pulse energy allows a depth resolved absorption measurement to a 2 km range with a $\frac{S}{N} = 1$, $n = 1$ and a 16 m depth resolution. The signal to noise ratio improves with increased transmitted energy but only as the square root of the number of averaged pulses. There is also a tradeoff in absorption sensitivity and depth resolution as

discussed previously. Obviously a number of the variables can be adjusted to improve the range and sensitivity of the differential absorption method. However, Fig. 10 shows that transmitted energies in the 10 mJ - 100 mJ range are necessary for differential absorption measurements in the infrared. The required energy is reduced somewhat in the visible due to increased scatter return and to more sensitive detectors. Examples of SO_2, NO_2 and I_2 detection are given by Measures and Pilon[5] and the required energy for NO_2 detection is discussed by Byer and Garbuny.[33]

The evaluation of the differential absorption method can be presented in an alternate way. If we assumed a fixed transmitted energy E_T, we can ask how the signal to noise ratio varies as a function of range. For a dark current limited detector we can invert Eq. (45) and solve for the S/N ratio to find

$$\frac{S}{N}(R) = E_T/E_o(R) \qquad x \ll 1$$

$$= 0.4\, E_T/E_o(R) \quad \sigma = \sigma_{opt} \tag{46}$$

where $x = 2 N_p L \sigma_{ABS}$ and $E_o(R)$ is given by Eq. (45) with S/N = 1.

Figure 11 shows the signal to noise vs range for the detection of CO using an InSb detector and for the detection of NO_2 using a photomultiplier detector. Hereit is assumed that the maximum S/N = 100 which corresponds to a measurement accuracy $\delta = \Delta R/R$ of 1%. For a 100 mJ transmitted pulse the signal to noise ratio decreases beyond 1 km leading to a decreasing measurement sensitivity with increasing range. For example, for both CO and NO_2 the minimum measurable concentration for a 15 m depth resolution is 0.14 ppm and 0.85 ppm which holds to a 1 km range for a 100 mJ transmitted pulse. At 2 km range the sensitivity is reduced to 1.4 ppm and 8.5 ppm. These sensitivities

can be improved by increasing the integration time and therefore the sampled depth and absorption length. However, care must be taken to adequately suppress the background power.

Schotland[122] has also considered errors involved in the differential absorption measurement due to parameters other than detector signal to noise ratio. These parameters include atmospheric properties, uncertainties in the absorption coefficient and laser frequency, and signal to noise limitations of the returned power measurement. Wright[120] has added digitization noise to the list of important contributions to the overall signal to noise ratio. However, as pointed out by Schotland,[122] it is ultimately the returned power signal to noise ratio which limits the range and accuracy of the differential absorption method. Within the past year experimental observations have verified the theoretically predicted parameters of the differential absorption method.

The earliest experimental work was performed by Schotland[118] who used a temperature tuned Ruby laser to measure the water vapor vertical profile by the differential absorption method. Using a cw 3.39 μm HeNe laser Granatstein et al.,[123] demonstrated differential absorption measurement of CH_4 and CO_2 in a controlled laboratory experiment. The first reported differential absorption measurements in the atmosphere were performed by Igarashi[119] who used a dye laser to probe for NO_2 over a 300m path. Concentrations of NO_2 and SO_2 were measured to 0.1 ppm over a 100m path using a 1 mJ dye laser transmitter.

Recently differential absorption measurements were considerably extended by Rothe, Brinkman and Walther[124,125] of Cologne, Germany. They used a 1 mJ, 30 nsec grating tuned dye laser operating between 4550 - 4700 $\mathring{A}$

for the tunable laser transmitter. This spectral region was chosen to include the more pronounced NO_2 absorption peaks. Following beam expansion the laser output was transmitted into the atmosphere and the backscattered signal was received with a 60 cm diameter Cassegrainian telescope and focused into a monochromator and onto a photomultiplier tube used in the photon counting mode. The differential range element was set at 500 m and ranges out to 3.75 km were probed. Concentrations as low as 0.2 ppm were detected over the city of Cologne.

The first calibration measurements of the differential absorption method were recently made by Grant et al.,[125] Using a flashlamp pumped dye laser operating near 4450 Å at 4-8 mJ pulse energy, Grant et al.,[125] measured NO_2 of known concentration in a sample chamber at 400 m range. Figure 12 shows the measurement results by the differential absorption method compared to the calibrated NO_2 concentration in the sample chamber. The uncertainty in the measurement is 20 ppm for a path length of 2.45 m at S/N = 1. This is equivalent to 0.5 ppm in 100 m path. The error analysis for this measurement includes consideration of power signal to noise, atmospheric conditions and digital processing error.

Perhaps the best demonstration of the differential absorption method is the two dimensional NO_2 density plot over a factory in the city of Cologne shown in Fig. 13. This composite of a series of range resolved measurements made by Rothe et al.,[126] illustrate the potential of the differential absorption measurement for pollution monitoring over urban areas. For these measurements nearly 2000 pulses of 1 mJ each were averaged. The range resolution is about 100 m. For the plot shown a total of 40,000 pulses were used at 1 Hz repetition rate.

To date the differential absorption method has been experimentally verified only in the visible spectral range. However, plans are underway in a number of research laboratories to carry out measurements in the infrared. For example Walther,[127] and Asai and Igarashi[128] are planning to use a TEA-CO_2 laser source for the detection of ozone near 10.4 μm. Also, work is being completed on a high energy 1.4 μm to 4.4 μm parametric tunable source[129] for application to near infrared differential absorption measurements. Based on previous experimental results in the visible, range resolved pollutant detection in the eye safe region of the infrared should prove to be a very useful monitoring tool in the near future.

III. CONCLUSION

The advances in the technology of tunable laser sources has opened new possibilities for the remote measurement of atmospheric pollutants. From the analysis and examples presented in Section II it is now possible to determine the required transmitted energy for each pollutant detection method and the sensitivity and range of the method at a given transmitted energy.

The Raman method, due to the very small Raman cross section, requires a fixed frequency laser of approximately 1 J per pulse energy to achieve even a minimal range and sensitivity. The lack of sensitivity, required operation in the visible region where eye safety is a serious problem, and the background and interference signals preclude the use of the Raman method for trace pollutant detection.

For local remote monitoring, the new four wave Raman mixing process which has scattering efficiencies 10^5 times that of spontaneous Raman scattering, looks very promising for trace gas analysis. However, experimental work

remains to be done to verify the sensitivity predictions.

The resonance and fluorescence backscatter detection methods require a tunable laser source as do the absorption methods. From the analysis of these remote detection methods it is apparent that the resonance and fluorescence backscatter method requires approximately 100 mJ of transmitted tunable energy for detection in the infrared. This high required energy, lack of depth resolution due to the long fluorescence decay times and variable cross section due to quenching, reduce the usefulness of the resonance method for remote monitoring in the troposphere. Only at high altitudes where quenching is not a problem and for atomic and molecular transisitons in the ultraviolet and visible does resonance backscatter offer detection advantages. For all other cases, the absorption methods are significantly better.

The absorption methods considered are long path absorption using a retroreflector or remote detector, long path absorption using a topographical target and the differential absorption method. For these methods the required power increases from approximately microwatts for the long path absorption method to pulsed energies of 1 mJ for the single ended topographical absorption method, to 10 to 100 mJ for the range resolved differential absorption method. For increased required tunable laser powers, the systems offer the advantages of single ended operation and single ended operation with depth resolution. The sensitivities of the three absorption methods are identical for equal path lengths.

The widespread use of the remote detection methods described in this paper depend critically upon the availability of narrow band, high energy tunable laser sources in the spectral region of interest.[130] Because of the molecular absorption spectra and the eye safety requirements the optimum

spectral range is in the 2 μm to 15 μm infrared region. It is only recently that tunable sources with adequate pulse energy have been demonstrated in the infrared. However, with the development of high pressure gas lasers[131] and high power nonlinear optical tunable sources,[132] the prospect for remote air pollution measurements looks brighter. In addition, the demonstration of diode laser operation in the infrared at liquid nitrogen temperatures[133] significantly extends the possibilities for their widespread use for long path absorption meausrements and as heterodyne detector local oscillators to improve the sensitivity of the topographical and differential absorption methods. With the improvement of tunable infrared laser sources, remote air pollution measurement should find wider application in the near future.

ACKNOWLEDGEMENTS

I want to acknowledge the support of NSF-RANN and NASA and the encouragement of Professor H. Inaba.

FIGURE CAPTIONS

1. Depth resolution for backscatter remote detection methods. The sampled depth is $\Delta R = c\tau/2$ where τ is the laser pulse width or detection integration time.

2. Detectable CO concentration vs range by the Raman backscattering method. Here a doubled Ruby laser source is assumed. The other parameters are discussed in the text.

3. a) Raman return from ordinary air at a range of 30 m for a 3371 Å transmitted beam from a pulsed nitrogen laser,

   b) Raman signal from an oil smoke showing the presence of H_2O, CH_4, H_2S, CO, NO and SO_2 (after Kobaysi and Inaba, ref. 75).

4. Fluorescence backscatter pollutant detection sensitivity vs range for CO in the infrared at 4.6 μm. A 100 mJ transmitted pulse is assumed and a single pulse (n=1) at S/N = 1 is evaluated. Sensitivities are shown for optically thin and optically thick pollutant layers.

5. a) Calculated heterodyne detection sensitivities of SO_2 using a CO_2 laser as a local oscillator vs the IF bandwidth-integration time product.

   b) Calculated heterodyne sensitivities for CO_2 detection assuming 100% irradiation of the detector (solid line) and 20% irradiation of the detector (dashed line) and measured sensitivity (crosses) for 20% detector irradiation. (After Menzies ref. 70).

6. Required transmitted energy vs range for CO detection at 4.7 μm. σ_{MAX} indicates tuning on line center and σ_{MIN} indicates tuning to the optimum cross section for minimum required energy. A 20 ppm CO cloud 100 m thick is assumed in the path. (After Byer and Garbuny, reference 33).

7. Minimum measurable pollutant concentration vs range at S/N = 100 for SO_2, NO_2 and CO. The parameters are similar to those assumed in Fig. 6 except for a shot noise limited photomultiplier detector with $F = 4$, $\Delta f = 20$ MHz and $\eta = 50\%$ for the SO_2 and NO_2 detection.

8. a) Vibrational-rotational overtone spectrum of CO by a tunable parametric laser. The measured cross section for CO at atmospheric pressure is 0.75×10^{-21} cm^2.

   b) Two rotational absorption lines in CO of 18 atm-cm optical density at 107 m distance. Zero transmission is presented by the small horozontal lines at the beginning and end of the trace (after Henningsen et al., reference 115).

9. Backscattered power vs range for detection of CO by the differential absorption method. $P_r^{off}(R)$ and $P_r^{on}(R)$ are the returned powers when tuned off and on the CO absorption line. Also shown is the logarithm of the ratio (dashed line) and the range derivative of $\ell n[P_r^{off}/P_r^{on}]$ which equals the CO pollutant concentration.

10. Required transmitted energy vs range for CO detection at 4.7 μm by the differential absorption method. For a 100 nsec resolvable pulse the depth resolution is 15 m and the minimum measurable pollutant concentration for S/N = 100 is 0.14 ppm.

11. S/N and measurement accuracy, δ, vs range for the differential absorption method assuming a 100 mJ, 100 nsec transmitted pulse. The depth resolution is 15 m. Here V is the visibility and σ_{MIN}, given by Eq. (43), is the optimum cross section.

12. A calibrated differential absorption measurement of NO_2 at 400 m. NO_2 measured by the differential absorption method vs NO_2 measured by transmissometer in the 2.45 m sample chamber. These measurements were taken at 4418 and 4448 $\mathring{A}$ (After Grant et al., reference 125).

13. NO_2 distribution over a chemical factory as derived from differential absorption measurements at the indicated directions at an altitude of 45 m . The concentratins are given in ppm (after Rothe et al., reference 126).

REFERENCES

1. H. Kildal and R.L. Byer, Proc. IEEE, vol. 59, p.1644, (1971).

2. V.E. Derr and C.G. Little, Applied Optics, 9, p.1976, (1970).

3. E.D. Hinkley and P.L. Kelley, Science, 171, p.635, (1971); see also I. Melngailis, IEEE, Trans. on Geo. Sic. Elect. GE-10, 1972.

4. H. Inaba and T. Kobayashi, Opto-Electronics, 4, p.101, (1972).

5. R.M. Measures and G. Pilon, Opto-Electronics, 4, p.141, (1972).

6. V.E. Derr, ed. Remote Sensing of the Troposphere, NOAA U.S. Government Printing Office, Washington, D.C. Cat. No. C55.602, T75, (1972).

7. L.B. Lane and E.P. Seskin, Science, 169, p.723, (1970).

8. G.B Morgan, G. Ozolins and E.C. Tabor, Science, 170, p.289, (1970).

9. G. Fiocco and L.D. Smullin, Nature, (London), 199, p.1275, (1963).

10. M.G.H Ligda, Proc. Conf. Laser Tech. 1st San Diego, California, U.S. Navy ONR, p.63, (1963).

11. H. Inaba, T. Kobayashi, T. Ichimura, Elect. and Comm. in Japan, vol. 51-B, p.36, (1968).

12. R.T.H. Collis in Advances in Geophysics, vol. 13, H E. Landsberg and J. van Mieghem, eds. (Academic Press Inc., N.Y. 1969), p.113.

13. G.S. Kent and R.W.H. Wright, J. Atm and Terrestrial Physics, vol. 32, p.917, (1970).

14. R.T.H. Collis, Appl. Optics, vol. 9, p.1782, (1970).

15. R.G. Strauch and A. Cohen, in Remote Sensing, ed. V. Derr, U.S. Department of Commerce, NOAA, August 15, 1972.

16. R.T.H. Collis and E.E. Uthe, Opto-Electronics, 4, p.87, (1972).

17. R.J. Allen and W.E. Evans, The Rev. of Sic, Inst. vol. 43, p.1422, (1972).

18. Freeman F. Hall, Jr. in Laser Applications, vol. 2, ed. by M. Ross, Academic Press, N.Y. 1974, p.161.

19. R.T. H. Collis and P.B. Russell, "Laser Applications in Remote Sensing", Stanford Research Institute, (to be published).

20. D.A. Leonard, Nature, vol. 216, p.142, (1967).

21. J.A. Cooney, Appl. Phys. Letts. vol. 12, p.40, (1968); see also J. Applied Meteorology, vol. 9, p.182, (1970).

22. S.H. Melfi, J.D. Lawrence, Jr. and M.P. McCormick, Appl. Phys. Letts. 15, p.295, (1969).

23. H. Inaba and T.Kobayashi, Nature, vol. 224, p.170, (1969); see also Opto-Electronics, 2, p.45, (1970).

24. T.Kobayashi and H. Inaba, Appl. Phys. Letts. 17, p.139, (1970).

25. J.A. Cooney, Journ. Appl. Meteorology, vol. 10, p.301, (1971).

26. R.G. Strauch, V.E. Derr and R.E. Cupp, Appl. Optics, vol. 12, p.2665, (1971).

27. S.H. Melfi, Appl. Optics, vol. 11, p.1605, (1972).

28. P.L. Hanst and J.A. Morreal, J. Air Pollut. Cont. Ass. vol. 18, p.754, (1968).

29. L.R. Snowman and R.J. Gillmeister, "Infrared Laser System for Extended Area Monitoring of Air Pollution", presented at the Joint Conference on Sensing of Environmental Pollutants, Palo Alto, California, 1971.

30. C.K.N. Patel, in Coherence and Quantum Optics, ed. by L. Mandel and E. Wolf, Plenum Press, Pub. Corp. N.Y. p.567, (1973).

31. R.T. Menzies and M.S. Shumate, Science, 184, p.570, (1974).

32. R.M. Schotland, Proc. of 3rd Int. Symp of Remote Environ. Sensing, (Univ. of Mich.), 1, p.273, (1966).

33. R.L. Byer and M. Garbuny, Appl. Optics, vol. 12, p.1496, (1973).

34. R. Penndorf, J. Opt. Soc. Am. 47, p.176, (1957).

35. R.F. Begley, A.B. Harvey and R.L. Byer, "Coherent Anti-Stokes Raman Spectroscopy", (to be published October 1, 1974, Appl. Phys. Letts.).

36. For Alternate Expressions of the Raman Cross Section in Terms of the Polarizability, see : G. Placzek, Handbook der Radiologie, (Adademishe Verlog, Leipzig 1934, ed. by E. Marx, vol. VI, part 2 ; E.J. Stansbury, M.F. Crawford and H.L. Welsh, Can. J. Phys. vol. 31, p.954, (1953) ; R.H. Pantell and H.E, Puthoff, Fundamentals of Quantum Electronics, John Wiley and Sons, N.Y. 1969 ; W. Kaiser and M. Maier, in Laser Handbook, ed. by F.T. Arecchi and E.O. Schulz - DuBois, vol. 2, North Holland Pub. Co. p.1077, (1972).

37. G. Mie, Ann. Physik, 25, 1908.

38. H.C. van de Hulst, Light Scattering by Small Particles, John Wiley and Sons, N.Y. 1957.

39. M. Kerker, The Scattering of Light, Academic Press, N.Y. 1969.

40. M. Born and E. Wolf, Principles of Optics, Pergamon Press, Oxford,1964.

41. R.W. Call, E. Palmer and R. Grow, "Light Scattering", University of Utah Tech. Report. NSF-11, (1967).

42. C.E. Junge, Air Chemistry and Radio Activity, Academic Press, N.Y, 1964.

43. L. Elterman, Environmental Research Paper No. 46, (Air Force Cambridge Research Labs. AFCRL-64-740, 1964).

44. A.E. Grimes, 1950-1969, ESSA Tech. Memo, ATSTM Lib 2 PB-188652, Springfield, Va. (1969).

45. L. Elterman, Appl. Optics, 9, p.1804, (1970).

46. P.W. Kruse, L.D. McGlauchlin and R.B. McQuistan, Elements of Infrared Technology, Wiley, N.Y. 1963.

47. S. Twomey and H.B. Howell, Appl. Opt. 4, p.501, (1965).

48. R.W. Fenn, Appl. Opt. 5, p.293, (1966).

49. A.Barnhart and J.L. Strete, Appl. Optics, vol. 9, p.1337, (1970).

50. D.B. Rensch and R.K. Long, Appl. Optics, vol, 9, p.1563, (1970).

51. R.A. Brodewie and W.C. Davis, Appl. Optics, vol. 11, p.1529, (1972).

52. R.M. Goody, Atmospheric Radiation, Oxford University Press, London. 1964.

53. K. Ya Kondratyev, Radiation in the Atmosphere, Academic Press, N.Y. 1969.

54. A.E.S. Green, The Middle Ultraviolet, New York, Wiley, 1966.

55. W.L. Wolfe, ed. Handbook of Military Infrared Technology, Office of Naval Research, U.S. Government Printing Office, Cat. No. 65-62266.

56. V.E. Derr, in Remote Sensing of the Troposphere, ed. by V.E. Derr, U.S. Government Printing Office, Cat. No. C55.602.T75.

57. S.F. Clifford, in Remote Sensing of the Troposphere, ed. by V. Derr, U.S. Government Printing Office, Cat. No. C55.602.T75.

58. J.P. Hansen and S. Madhu, "Appl. Optics, 11, p.233, (1972).

59. W.F. Dabberdt and W.B. Johnson, Appl. Optics, 12, p.1544, (1973).

60. W.K. Pratt, Laser Communication Systems, New York, Wiley, 1969.

61. For example refer to Operation of a Geodolite System Manufactured by Spectra Physics, Inc., Mountain View, California.

62. M.C. Teich, Proc. IEEE, vol. 56, p.37, (1968).

63. F.R. Arams, E.W. Sard, B.J. Peyton and F.P. Pace, IEEE, Journ. Quant. Elect. vol. QE-3, p.484, (1967).

64. E.D. Hinkley and R.H. Kingston, Proc. of the Joint Conference on Sensing of Environmental Pollutants, Palo Alto, California. 8-10 November 1971.

65. E.D. Hinkley, Opto-Electronics, 4, p.69, (1972).

66. A.E. Sigeman, Appl. Optics, 5, p.1588, (1966).

67. D.A. Kleinman and G.D. Boyd, Journ. Appl. Physics, 40, p.546, (1969).

68, H.A. Smith and H. Mahr, "An Infrared Detector for Astronomy Using Up-Conversion Techniques", presented at the International Quantum Electronics Conference, Kyoto, Japan, September 1970.

69. R.T. Menzies, Appl. Optics, vol. 10, p.1532, (1971).

70. R.T. Menzies, Opto-Electronics, 4, p.179, (1972).

71. R.L. Byer, Chromatix Technical Note No. 4, Chromatix Inc., Mountain View, California.

72. R.D. Compton, ed. Electro-Optical Systems Design, vol. 6, p.20, (May 1974).

73. L.R. Lidholt, Opto-Electronics, 4, p.133, (1972).

74. H.A. Hyatt, J.M. Cherlow, W.R. Fenner and S.P.S. Porto, Journ. Opt. Soc. Am. 63, p.1604, (1973).

75. T.Kobayashi and H.Inaba, "Laser Beam Technology for Remotely Sensing Invisible Molecules in the Polluted Atmosphere", 11th Symposium on Electron, Ion and Laser Beam Technology, ed. R.F.M. Thornley, San Francisco Press, Inc., p.385, (1971); see also S. Nakahara, K. Ito, S. Ito, A. Fuke, S. Komatsu, H. Inaba and T.Kobayashi, Opto-Electronics, 4, p.169, (1972).

76. J.A. Cooney, Journ. Appl. Meteorology, 12, p.888, (1974).

77. T. Hirschfeld, E.R. Schildleraut, H. Tannenbaum and D. Tannenbaum, Appl. Phys. Letts. 22, p.38, (1973); see also T. Hirschfeld and S. Klainer, Optical Spectra, p.63, (July 1970).

78. T. Hirschfeld, Appl. Optics, 13, p.1435, (1974).

79. G.S. Kent, P. Sandland and R.W. Wright, J. Appl. Meteorology, 10, p.443, (1971).

80. M.J. Garvey and G.S. Kent, Nature, 248, p.124, (1974).

81. P.D. Maker and R.W. Terhune, Phys. Rev. 137, p.A801, (1965).

82. R.L. Schwiesow, in Remote Sensing, ed. V. Derr, U.S. Department of Commerce, NOAA, August,15, 1972, (Cat. No. C55-602 : T75) ; see also O.S. Mortensen, Mol. Phys. vol. 22, p.179, (1971).

83. M. Rokni and S. Yatsiv, Phys. Letts. 24A, p.277, (1967).

84. D.G. Fouche and R.K. Chang, Phys. Rev. Letts. 29, p.536, (1972); see also R.L. St. Peters, S.D. Silverstein, M. Lapp and D.M. Penney, Phys. Rev. Letts. 30, p.191, (1973).

85. P F. Williams and D.L. Rousseau, Phys. Rev. Letts. 30, p.951, (1973).

86. W. Holzer, W.F. Murphy and H.J. Bernstein, J. Chem. Phys. 52, p.399 and p.469, (1970); see also, W. Kieffer and H.J. Bernstein, Journ. Mol. Spectroscopy, 43, p.366, (1972).

87. P.R. Fenstermacher and R.H. Callender, Optic Comm. 10, p.181, (1974).

88. Wm. H. Smith, Opto-Electronics, 4, p.161, (1972).

89. J.J. Barrett and S.A. Myers, Journ. Opt. Soc. Am. 61, p.1246, (1971).

90. R.F. Begley, A.B. Harvey, R.L. Byer and B.S. Hudson, "A New Spectroscopic Tool:Coherent Anti-Stokes Raman Spectroscopy", American Laboratory, (November 1974), to be published.

91. P.R. Regnier and J.P.E. Taran, "Gas Concentration Measurement by Coherent Raman Anti-Stokes Scattering", AIAA 6th Fluid and Plasma Dynamics Conference, Palm Springs, California, July 16-18, 1973; see also P.R. Regnier and J.P.E. Taran, Appl. Phys. Letts. 23, p.240, (1973).

92. M.R. Bowman, A.J. Gibson and M.C.W. Sandford, Nature, vol. 221, p.456, (1969); see also A.J. Gibson, Journ. Sci. Instr. vol. 2, p.802, (1969).

93. M.C.W. Sandford and A.J. Gibson, J. Atmos. Terr. Phys. 32, p.1423, (1970).

94. A.J. Gibson and M.C.W. Sandford, J. Atmos. Terr. Phys. 33, p.1675, (1971).

95. C.J. Schuler, C.T. Pike and H.A, Miranda, Appl. Opt. 10, p.1689, (1971).

96. R.D. Hake, D.E. Arnold, D.W. Jackson, W.E. Evans, B.P. Ficklin and R.A. Long, J. Geophys. Res. 77, p.6839, (1972).

97. J.E. Blamont, M.L. Chanin and G. Megie, Ann. Geophys. 28, p.833, (1973).

98. V.W.J.H. Kirchoff and B.R. Clemesha, J. Atm. Terr. Phys. 35, p.1493,(1973).

99. A.J. Gibson and M C.W. Sandford, Nature 239, p.509, (1972).

100. F. Felix, W. Keenliside, G. Kent and M.C.W. Sandford, Nature 246, p.345, (1973).

101. C.M. Penney, W.W. Morey, R.L. St. Peters, S.D. Silverstein, M. Lapp and D.R. White, Final Report for NASA CR-132363, prepared by General Electric Corporate Research and Development, Schenectady, New York.

102. O. Stern and M. Volmer, Phys. Z. vol. 20, p.183, (1919).

103. J.A. Gelbwachs, M. Birnbaum, A.W. Tucker, C.L. Fincher, Opto-Electronics, 4, p.155, (1972).

104. J.M. Taylor and H.W. Yates, J. Opt. Soc. Am. 47, p.223, (1957); see also G.S. Newcomb and M.M. Milan, IEEE Trans. Geo. Sic. Elect. GE-8, p.149,(1970).

105. A.R. Barringer and B.C. Newbury, Ninth Conference, Air Pollution and Industrial Hygiene Studies, Pasadena, California, February 1968.

106. G.B. Jacobs and L.R. Snowman, IEEE Journ. Quant. Elect. vol. QE-3, p.603, (1967).

107. P.L. Hanst, Appl. Spectros. 24, p.161, (1970).

108. S. Zaromb, Proc. Electro-Optical Systems Design, Symposium, p.609, September 1969.

109. S. Nakahara and K. Ito, International Quantum Electronics Conference Digest Tech. Papers, p.226, September 1970.

110. H. Inomata and T. Igarashi, Trans. Technical Group on Quant. Elect. of the Inst. Elect. Comm. Eng. (IECE) of Japan, QE-70 - 36, December 1970, (in Japanese).

111. J.A. Hodgeson, W.A. McClenney, P.L. Hanst, Science, vol. 182, p.248, (1973).

112. E.D. Hinkley, Appl. Phys. Letts. vol. 16, p.351, (1970); see also K.W. Nill, F.A. Blum. A.R. Calawa and T.C. Harman, Appl. Phys. Letts. 19, p.79, (1971).

113. L.R. Snowman, Technical Report R72ELS-15, General Electric Electronic Laboratory, Syracuse, New York, March 1972.

114. D. O'Shea and L.G. Dodge, Appl. Optics, 13, p.1481, (1974).

115. T. Henningsen, M. Garbuny and R.L. Byer, Appl. Phys. Letts. 24, p.242, (1974).

116. T.H. Maugh II, Science, 177, p.338, (1972).

117. E.D. Hinkley, "The Use of Tunable Lasers in Infrared Atmospheric Spectroscopy", Fifth Conference on Laser Radar Studies of the Atm, Williamsburg, Va. June 4-6, 1973.

118. R.M. Schotland, E.E. Chermack and D.T. Chang, Proc. First International Symp. of Humidity and Moisture, p.569, (Reinhold Book Div. New York, N.Y. 1964); see also R.M. Schotland, Proc. Third Symp. on Remote Sensing of the Environment, p.215, October 14-16, 1964, Univ. of Michigan, Ann Arbor, Mich.

119. T. Igarashi, "Laser Radar Study Using Resonance Absorption for Remote Detection of Air Pollutants", Fifth Conference on Laser Radar Studies of the Atm, June 4-6, 1973, Williamsburg, Va.

120. M.L. Wright, Stanford Research Institute, Menlo Park, California, (private communication).

121. H. Inaba, T.Kobayashi, T. Ichimura, M. Morihisa and K. Taira, Elect. and Communications in Japan, vol. 51-B, p.45, (1968).

122. R.M. Schotland, Journ. Appl. Meteorology, 13, p.71, (1974).

123. V.L. Granastein, M. Rhinewine and A.H. Fitch, Appl. Opt. 12, p.1511, (1973).

124. K.W. Rothe, U. Brinkmann and H. Walther, Proc. VIII ICPEAC, Beograd, (July 1973); see also, Appl. Phys. 3, p.115, (1974).

125. W.B. Grant, R.D. Hake Jr. E.M. Liston, R.C. Robbins and E.K. Proctor, Jr. Appl. Phys. Letts. 24, p.550, (1974).

126. K.W. Rothe, U. Brinkman, H. Walther, "Remote Measurement of NO_2 Emission from a Chemical Factory by the Differential Absorption Technique", (to be published in Applied Physics).

127. H. Walther, (private communication).

128. K. Asai and T. Igarashi, "Detection of Ozone in the Atmosphere Using Differential Absorption Technique with CO_2 Laser", submitted to Inter. Conference on Optical Methods, Tokyo, Japan, August 26-30, 1974.

129. R.L. Herbst, R.N. Fleming and R.L. Byer, "A 1.4 μm to 4 μm High Energy Angle Tuned $LiNbO_3$ Parametric Oscillator", (to be published).

130. J. Kuhl and W. Schmidt, Appl. Phys. 3, p.251, (1974).

131. O.R. Wood, II, Proc. IEEE, vol. 62, p.355, (1974).

132. R.L. Byer in Annual Review of Materials Science, vol. 4, p.147, (1974).

133. E.D. Hinkley, (private communication).

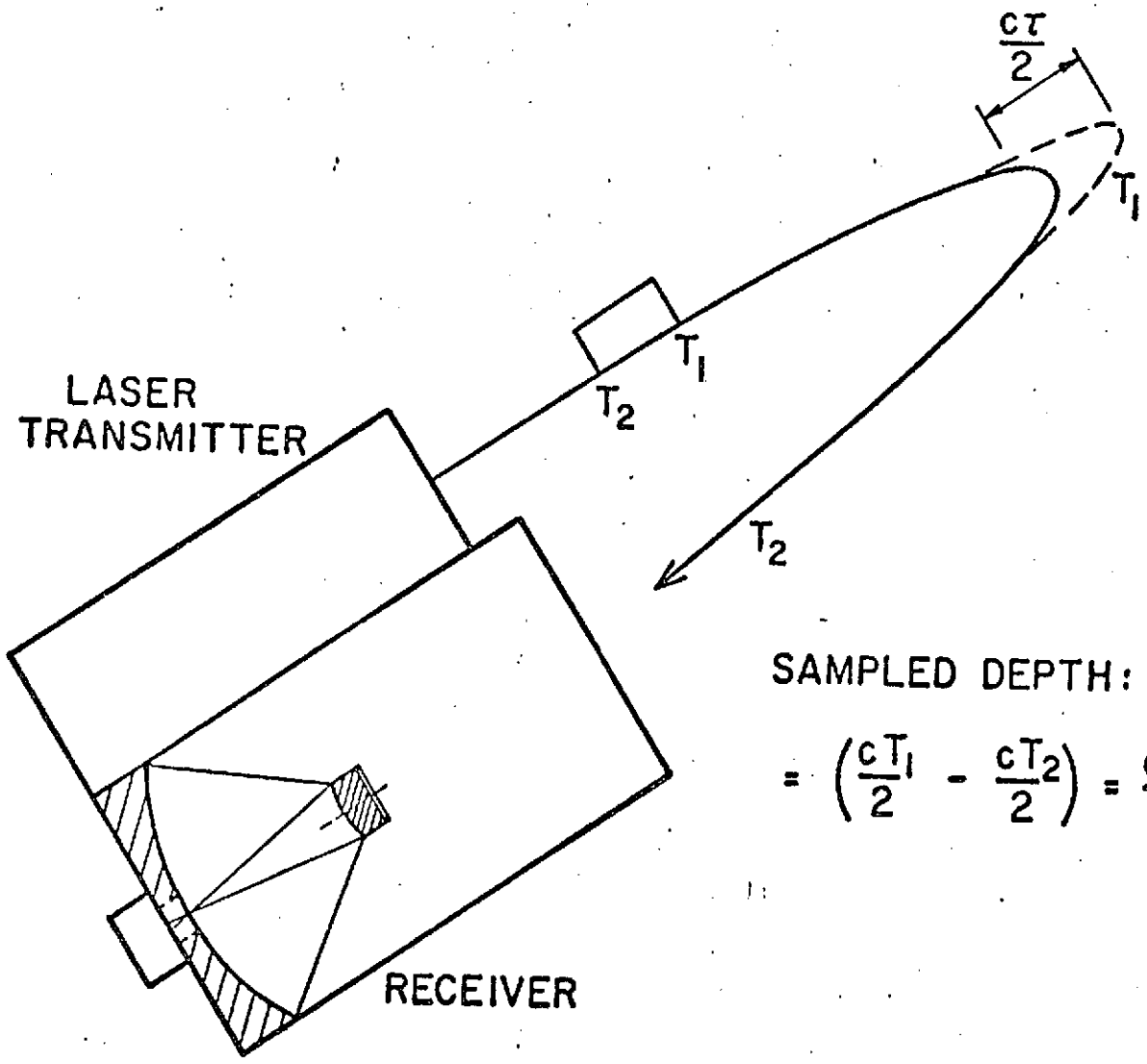

SAMPLED DEPTH:

$$= \left(\frac{cT_1}{2} - \frac{cT_2}{2}\right) = \frac{c\tau}{2}$$

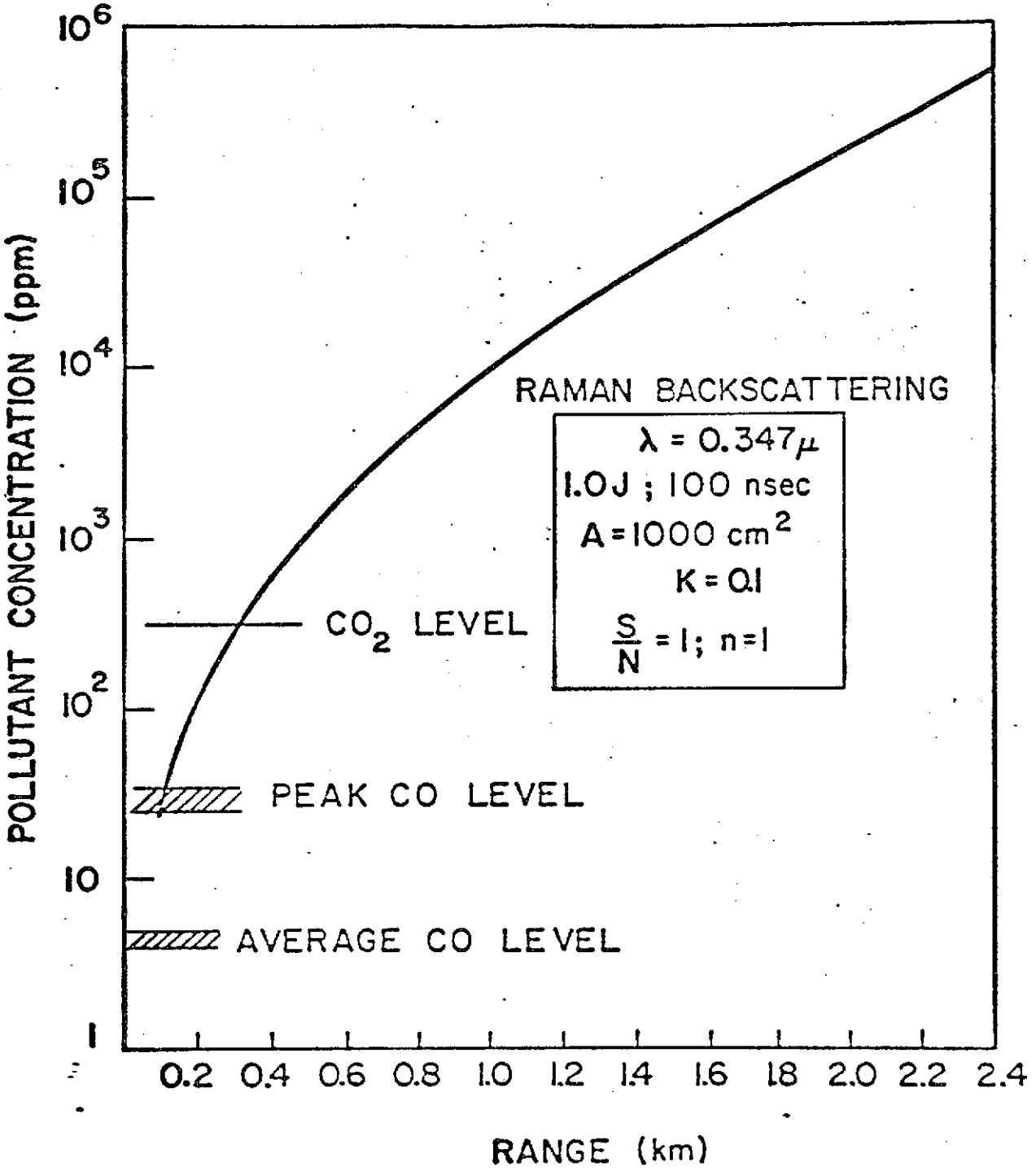
POLLUTANT CONCENTRATION (ppm)
10^6
10^5
10^4
10^3
10^2
10
1
RAMAN BACKSCATTERING
λ = 0.347μ
1.0J ; 100 nsec
A = 1000 cm²
K = 0.1
S/N = 1; n=1
CO₂ LEVEL
PEAK CO LEVEL
AVERAGE CO LEVEL
0.2 0.4 0.6 0.8 1.0 1.2 1.4 1.6 1.8 2.0 2.2 2.4
RANGE (km)

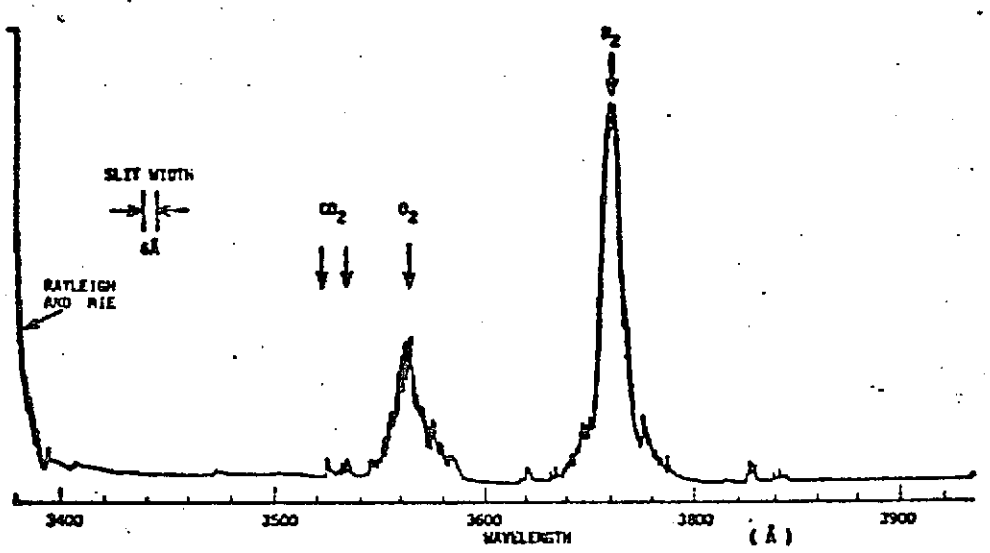
SLIT WIDTH
6Å
CO_2
O_2
N_2
RAYLEIGH AND NIE
3400
3500
3600
3800
3900
WAVELENGTH (Å)

(a)

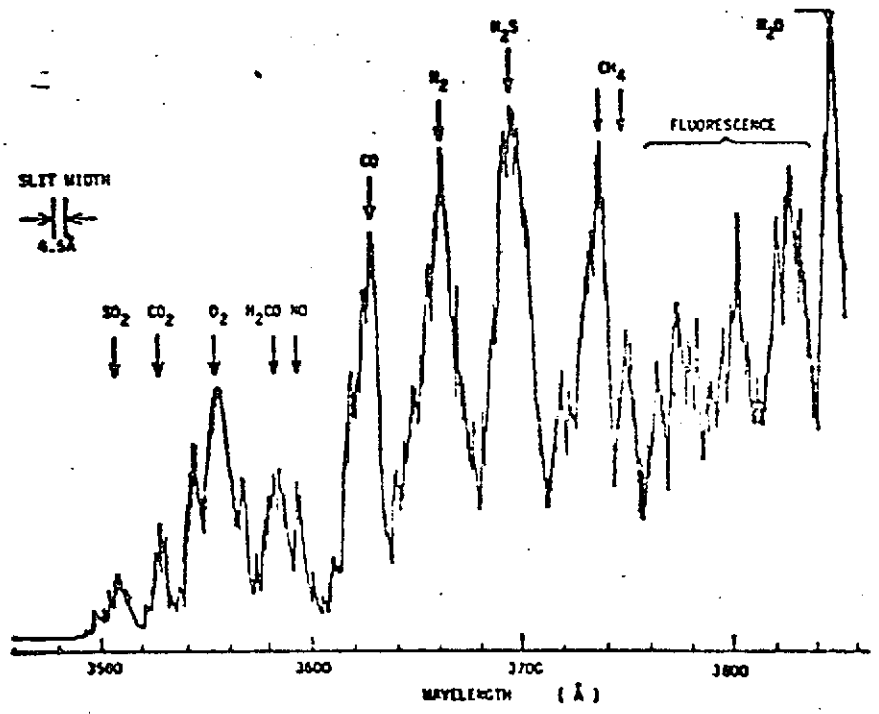
SLIT WIDTH
4.5Å
SO_2
CO_2
O_2
H_2CO
NO
CO
N_2
H_2S
CH_4
H_2O
FLUORESCENCE
3500
3600
3700
3800
WAVELENGTH (Å)

(b)

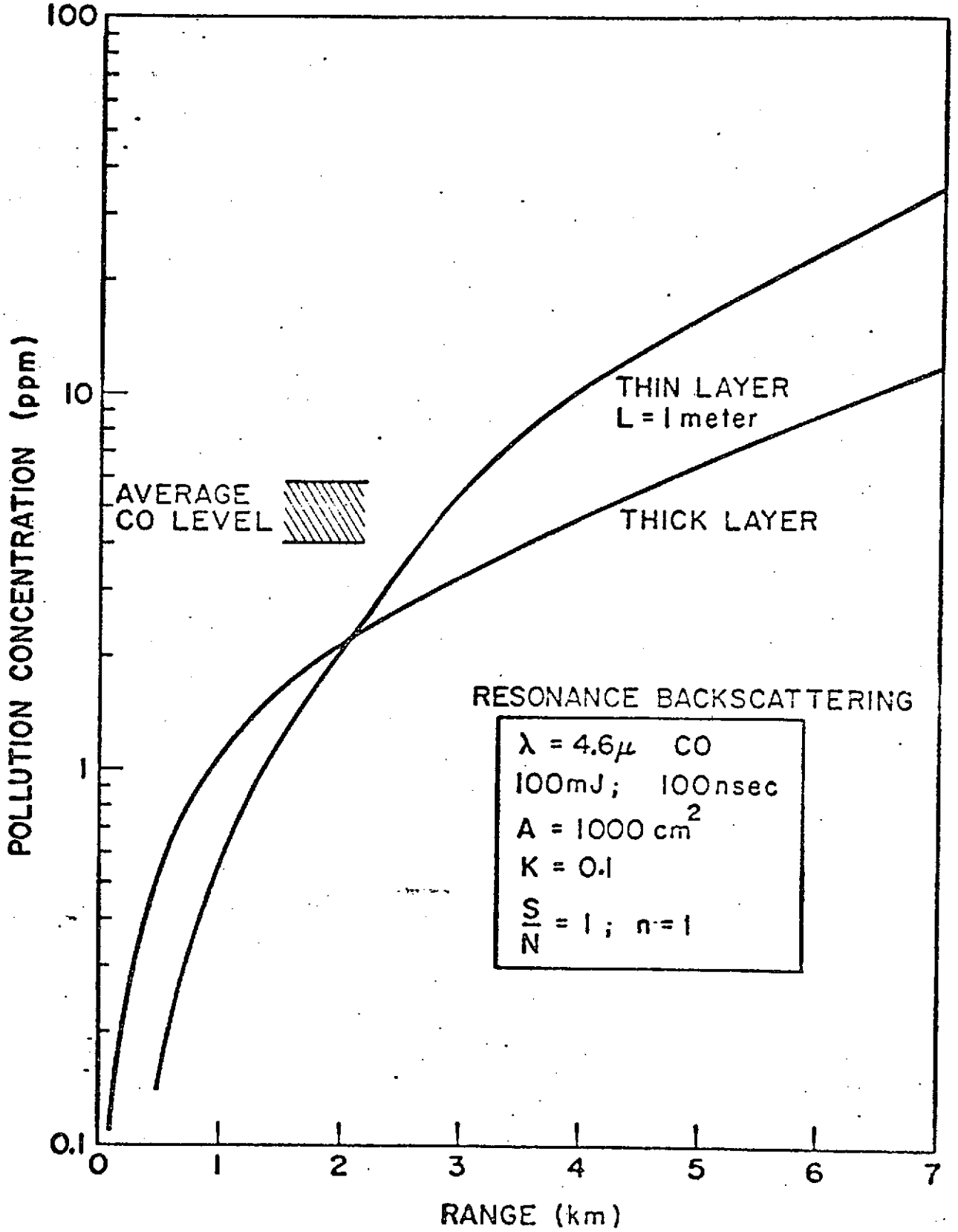
100
10
1
0.1
POLLUTION CONCENTRATION (ppm)
AVERAGE
CO LEVEL
THIN LAYER
L = 1 meter
THICK LAYER
RESONANCE BACKSCATTERING
λ = 4.6μ CO
100mJ; 100nsec
A = 1000 cm²
K = 0.1
S/N = 1; n = 1
0
1
2
3
4
5
6
7
RANGE (km)

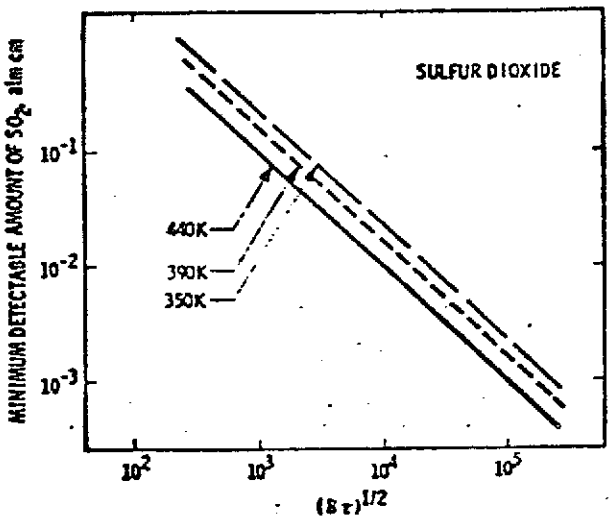
SULFUR DIOXIDE
MINIMUM DETECTABLE AMOUNT OF SO_2, atm cm
10^{-1}
10^{-2}
10^{-3}
440K
390K
350K
10^2
10^3
10^4
10^5
$(B\tau)^{1/2}$

(a)

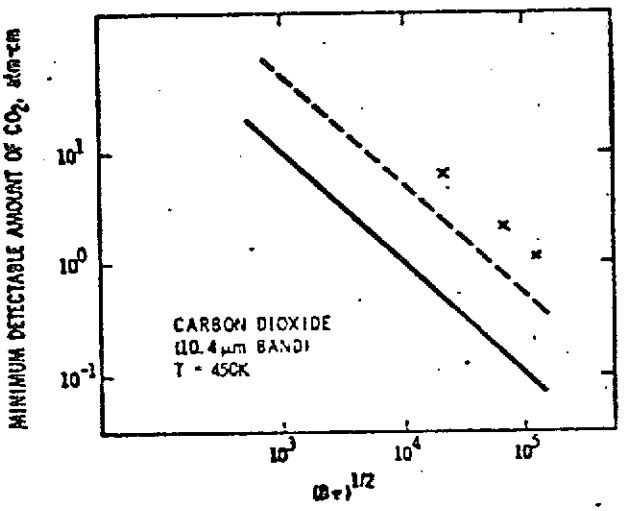
MINIMUM DETECTABLE AMOUNT OF CO_2, atm-cm
10^1
10^0
10^{-1}
CARBON DIOXIDE
(10.4 μm BAND)
T = 450K
10^3
10^4
10^5
$(B\tau)^{1/2}$

(b)

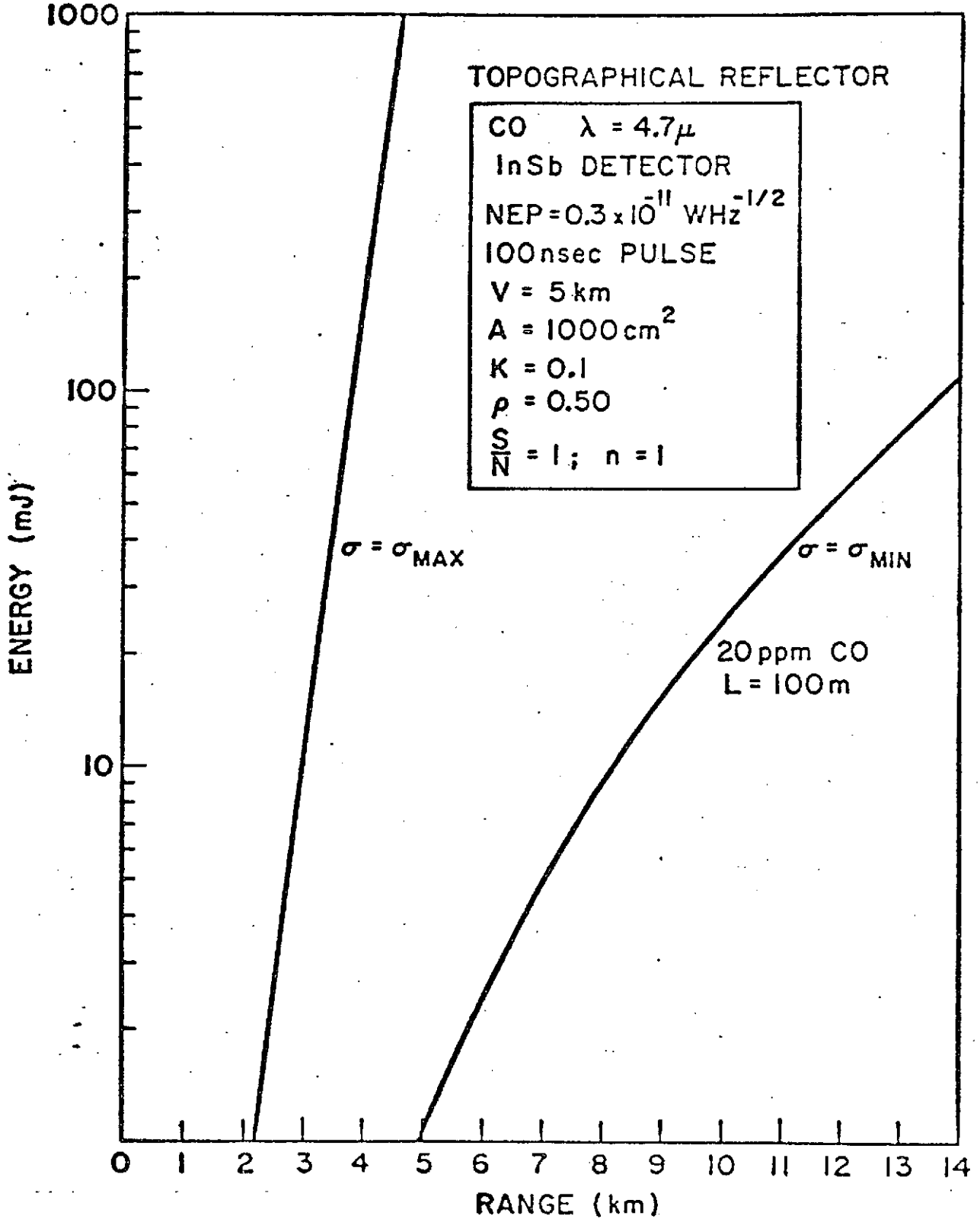
TOPOGRAPHICAL REFLECTOR
CO λ = 4.7μ
InSb DETECTOR
NEP = 0.3 x 10^-11 WHz^-1/2
100nsec PULSE
V = 5 km
A = 1000 cm^2
K = 0.1
ρ = 0.50
S/N = 1; n = 1
σ = σMAX
σ = σMIN
20 ppm CO
L = 100 m
ENERGY (mJ)
1000
100
10
0 1 2 3 4 5 6 7 8 9 10 11 12 13 14
RANGE (km)

C-2

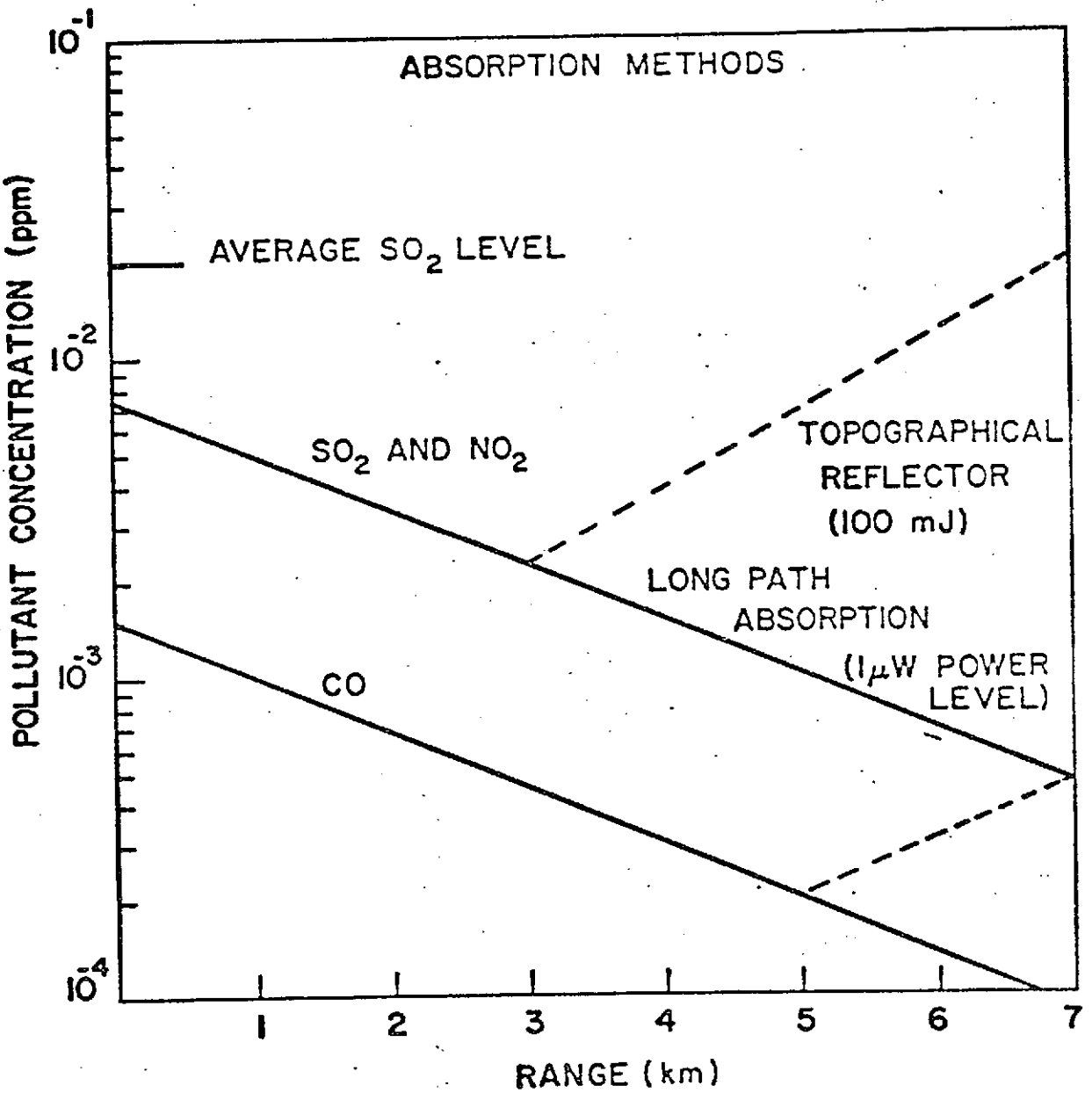
ABSORPTION METHODS
AVERAGE SO_2 LEVEL
SO_2 AND NO_2
CO
TOPOGRAPHICAL REFLECTOR (100 mJ)
LONG PATH ABSORPTION (1μW POWER LEVEL)
POLLUTANT CONCENTRATION (ppm)
10^{-1}
10^{-2}
10^{-3}
10^{-4}
1
2
3
4
5
6
7
RANGE (km)

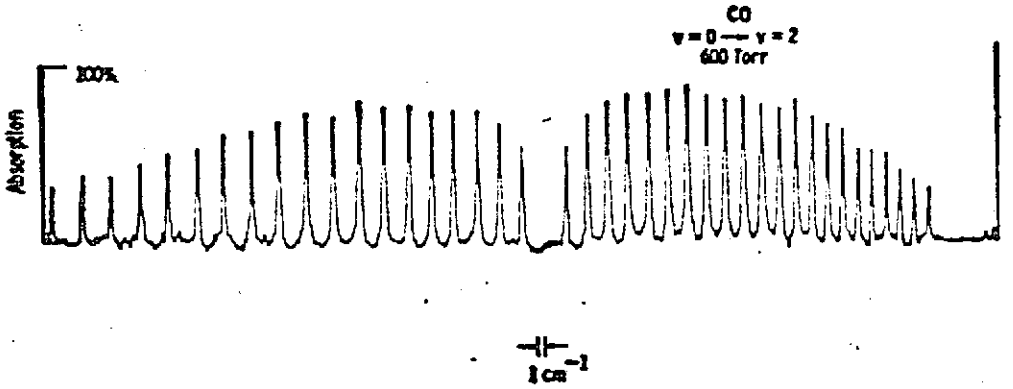

(a)

(b)

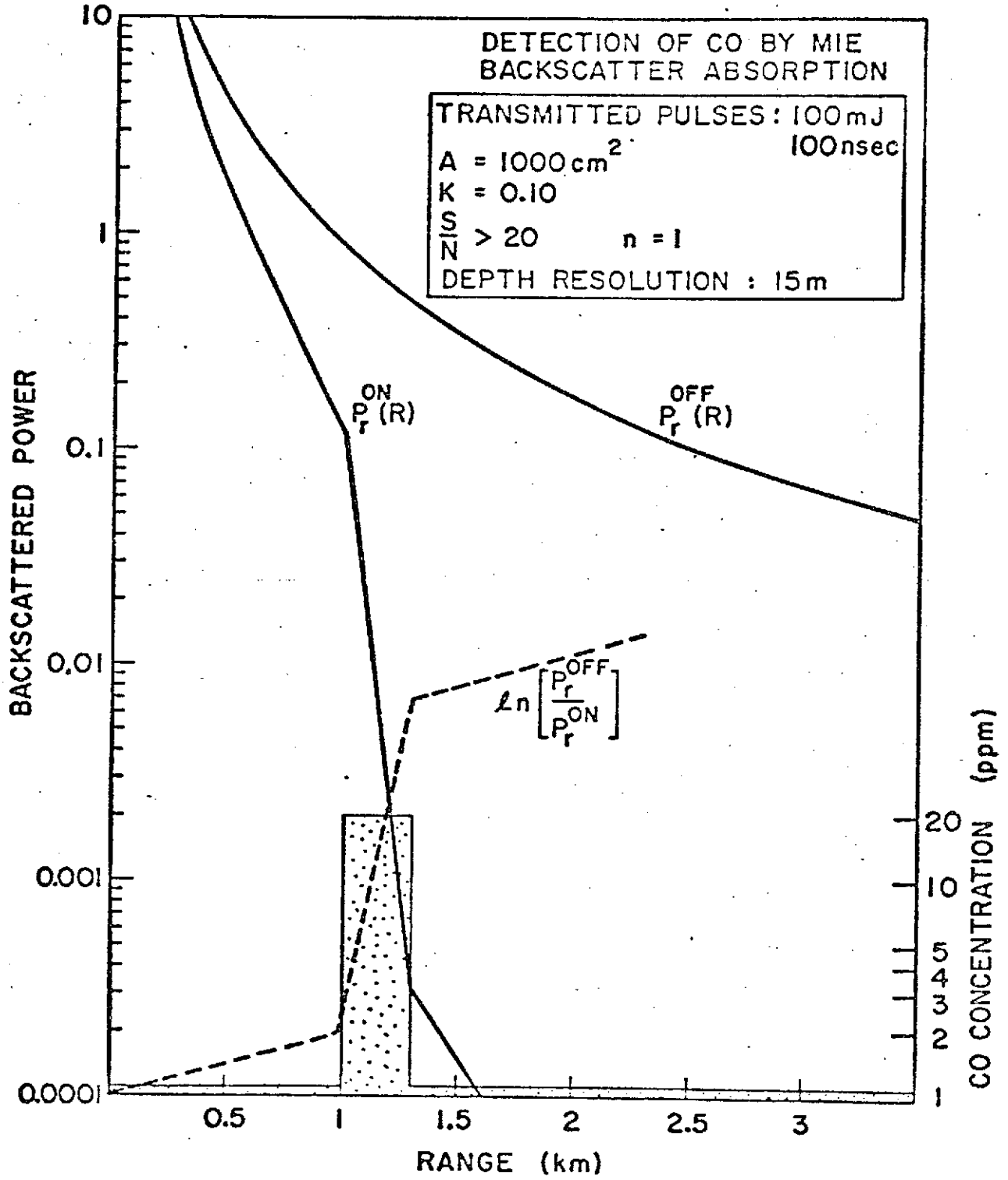
DETECTION OF CO BY MIE
BACKSCATTER ABSORPTION
TRANSMITTED PULSES : 100 mJ
100 nsec
A = 1000 cm²
K = 0.10
S/N > 20
n = 1
DEPTH RESOLUTION : 15 m
$P_r^{ON}(R)$
$P_r^{OFF}(R)$
$\ell n \left[\frac{P_r^{OFF}}{P_r^{ON}}\right]$
BACKSCATTERED POWER
10
1
0.1
0.01
0.001
0.0001
0.5
1
1.5
2
2.5
3
RANGE (km)
20
10
5
4
3
2
1
CO CONCENTRATION (ppm)

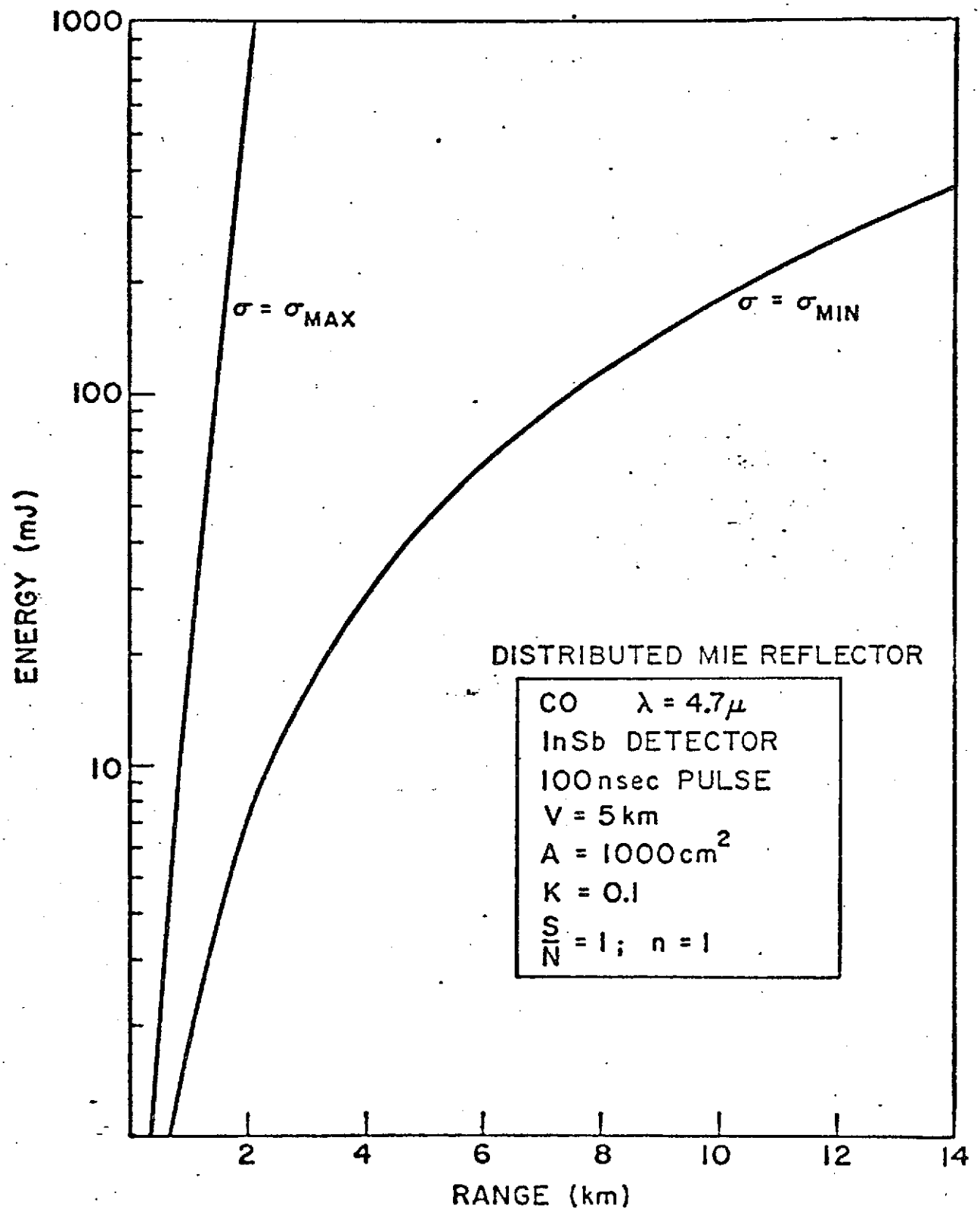
1000
100
10
ENERGY (mJ)
σ = σMAX
σ = σMIN
DISTRIBUTED MIE REFLECTOR
CO λ = 4.7μ
InSb DETECTOR
100nsec PULSE
V = 5km
A = 1000cm²
K = 0.1
S/N = 1; n = 1
2
4
6
8
10
12
14
RANGE (km)

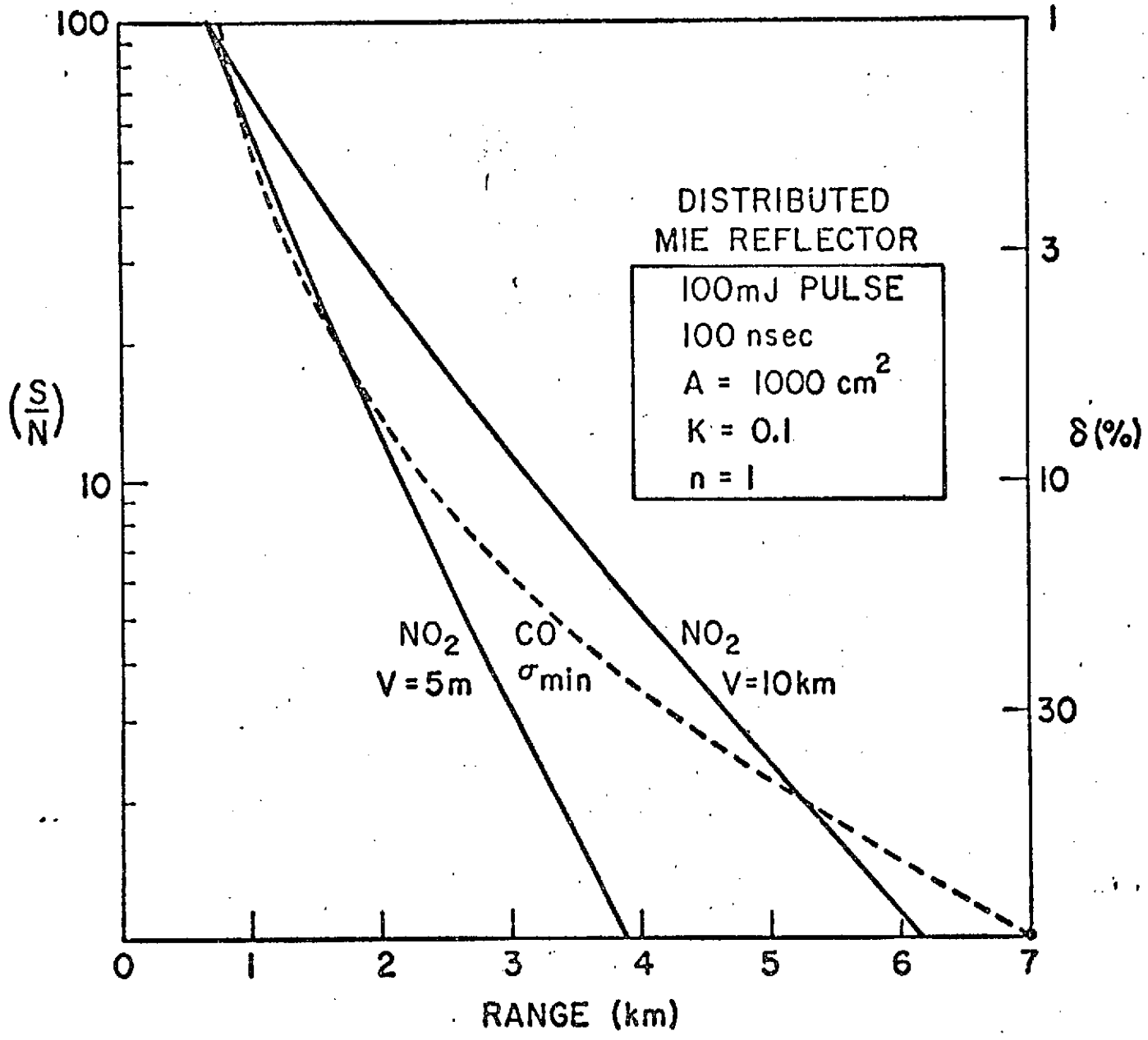
100
10
1
3
10
30
$\left(\frac{S}{N}\right)$
δ(%)
DISTRIBUTED
MIE REFLECTOR
100mJ PULSE
100 nsec
A = 1000 cm²
K = 0.1
n = 1
NO₂
V = 5m
CO
σmin
NO₂
V = 10km
0
1
2
3
4
5
6
7
RANGE (km)

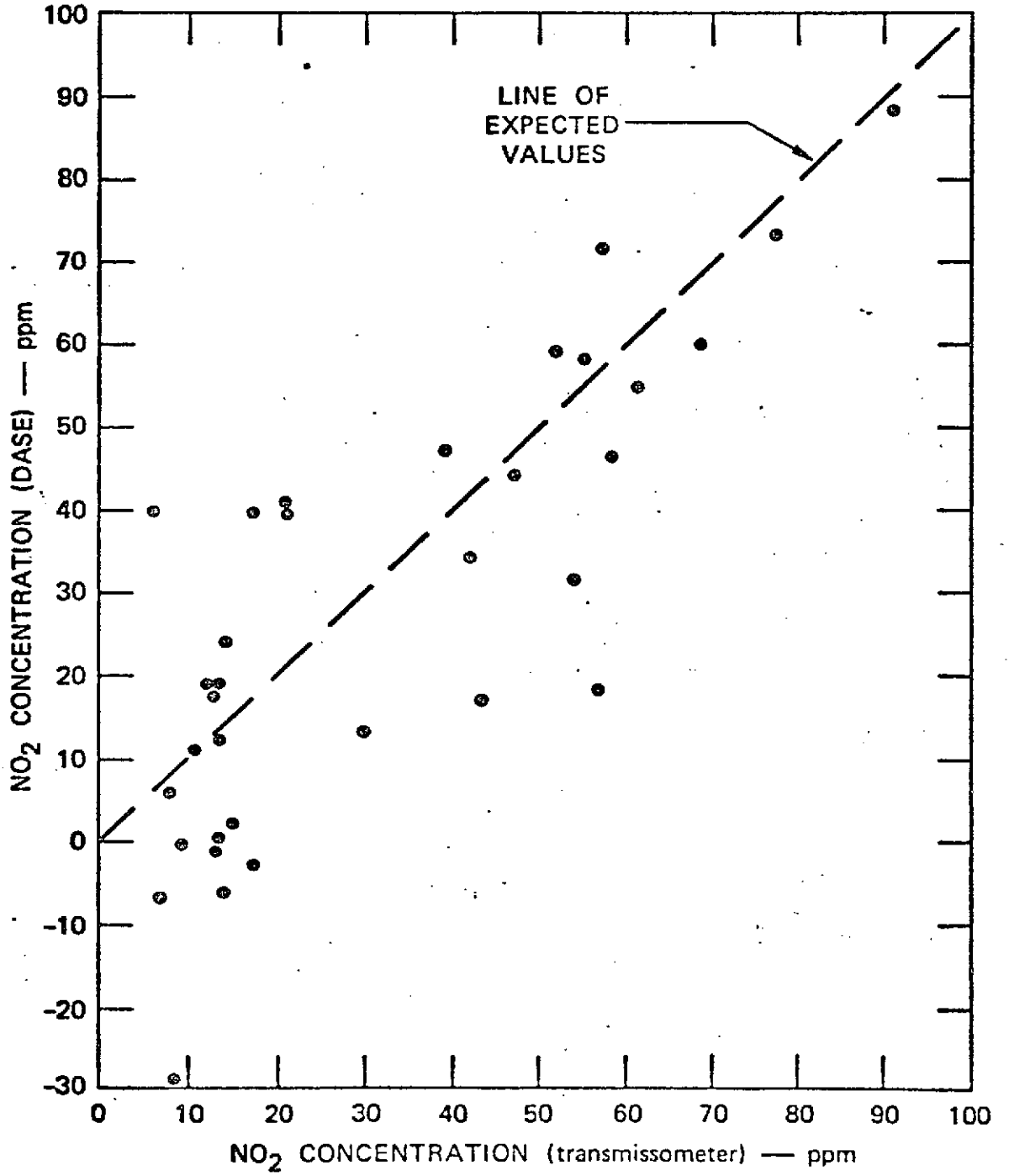
LINE OF EXPECTED VALUES
100
90
80
70
60
50
40
30
20
10
0
-10
-20
-30
0
10
20
30
40
50
60
70
80
90
100
NO2 CONCENTRATION (DASE) — ppm
NO2 CONCENTRATION (transmissometer) — ppm

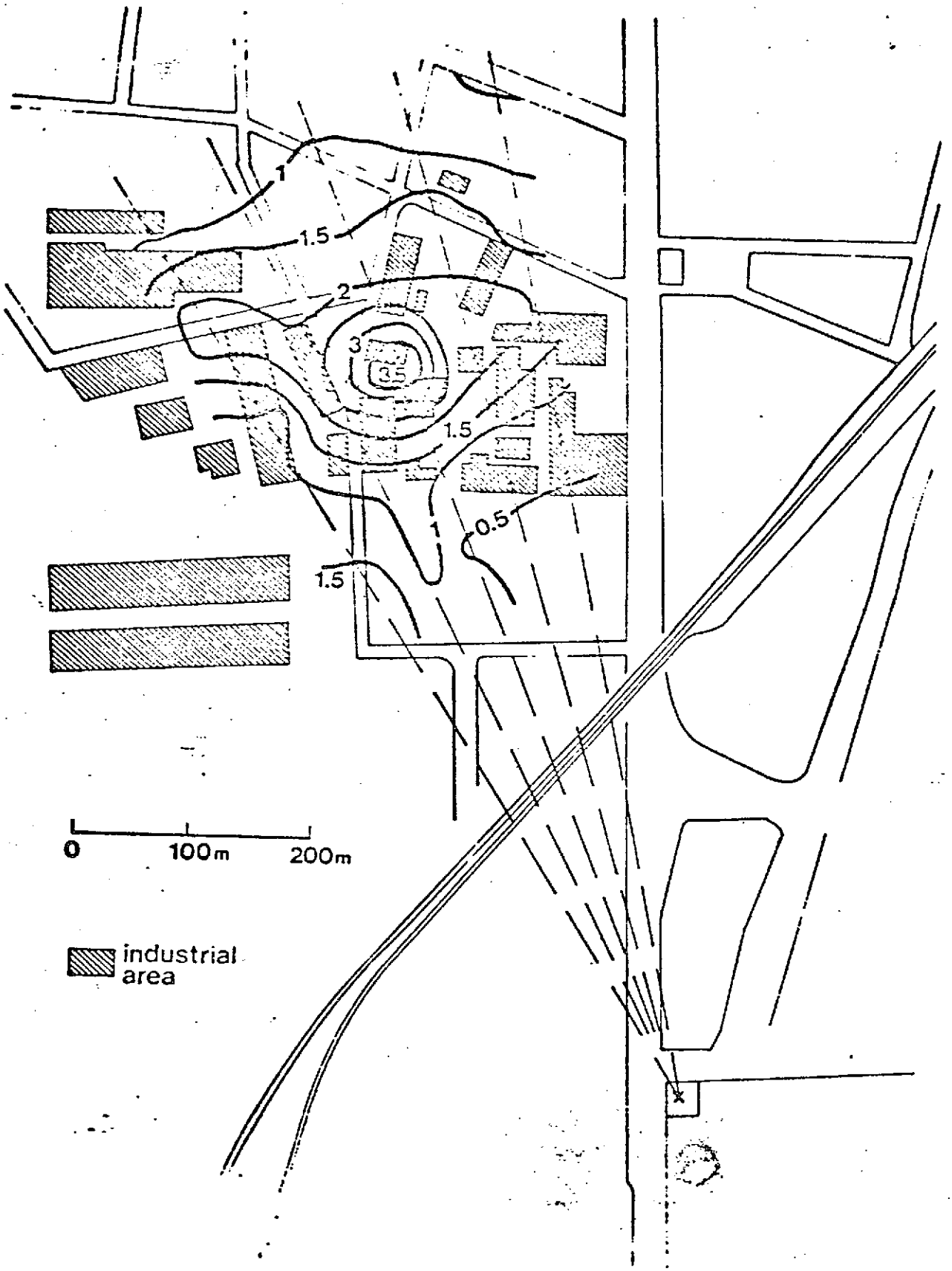
1
1.5
2
3
3.5
1.5
1
0.5
1.5
0
100m
200m
industrial area